DEFENCE
SCIENCE & TECHNOLOGY

Shape Optimisation of Two Closely-Spaced Holes for Fatigue Life Extension

W. Waldman, M. Heller and
L.R.F. Rose

DSTO-RR-0253

DEFENCE
SCIENCE & TECHNOLOGY

Shape Optimisation of Two Closely-Spaced Holes for Fatigue Life Extension

W. Waldman, M. Heller and L.R.F. Rose

Air Vehicles Division
Platforms Sciences Laboratory

DSTO-RR-0253

ABSTRACT

This report presents a set of free-form optimal shapes and the corresponding stress concentration factors for two interacting closely-spaced holes in a large biaxially loaded plate. A range of interaction distances and two distinct biaxial loading cases are considered, namely tensile field (remote principal stresses have the same sign) or mixed field (remote principal stresses have the opposite sign). The optimal shapes are obtained using the finite element analysis based gradientless shape optimisation method recently developed in AVD. In a key unexpected result, which has not previously been identified, it has been discovered that the peak stress associated with the optimal holes is independent of the interaction distance, and that the peak stress is the same as that for an optimal single hole. In both stress field cases, the absolute value of the tangential stress is piecewise constant around the hole boundary. Compared to interacting closely-spaced circular holes, which are a common feature in aircraft structures producing significant stress concentrations that often lead to premature fatigue cracking, the optimal hole shapes provide for very large reductions in peak stress (typically greater than 30%), which results in a substantial increase in fatigue life. The free-form optimal shapes are presented in a tabular form that allows them to be used readily by designers. For the tensile biaxial field, the optimal shapes are smooth and non-circular. For the mixed biaxial field case, the optimal shapes are approximately rectangular with sharp corners and curved sides, and no stress singularities are present at the corners.

RELEASE LIMITATION

Approved for public release

Published by

DSTO Platforms Sciences Laboratory
506 Lorimer Street
Fishermans Bend VIC 3207
Australia

Telephone: (03) 9626-7000
Fax: (03) 9626-7999

AR-012-771
May 2003

APPROVED FOR PUBLIC RELEASE

Shape Optimisation of Two Closely-Spaced Holes for Fatigue Life Extension

Executive Summary

In recent years, Air Vehicles Division (AVD) has been undertaking research to improve the capability to optimise the precise free-form shapes of holes and fillets, in the context of life extension of ageing RAAF aircraft components. Here the approach is to precisely reshape the holes to an optimal shape that minimises the magnitude of the peak stresses on the hole boundary, and thereby inhibits the formation of fatigue cracks. The application of such optimal shapes to RAAF aircraft components can provide large savings in the cost of ownership, through an extension of the time intervals between costly inspections. For example, a notable recent application is the shape optimisation of holes in the F-111 wing pivot fitting. While there has been significant progress to date in this topic, there are certain technical issues that need to be addressed to derive the most benefit from the shape optimisation approach. One such issue is the effect of interacting closely-spaced holes, which are a very common feature in RAAF aircraft. Typically, standard circular holes are non-optimal and result in significant stress concentrations, which can lead to undesirable fatigue cracking in components early in their service life. In addition, there are no published solutions for optimal hole shapes that could offer a practicable alternative to the use of circular holes.

This report presents practical solutions to the problem of determining optimal hole shapes for two closely-spaced holes in a large biaxially loaded plate. During this work, enhancements to the recently developed AVD finite element based gradientless shape optimisation procedure have been implemented. Two distinct biaxial loading cases are considered, namely tensile field (remote principal stresses have the same sign) or mixed field (remote principal stresses have the opposite sign). The resulting free-form optimal shapes provide very large reductions in stress (typically greater than 30%), as compared to the initial circular holes. For the tensile field, the solution shape is smooth and non-circular, and the stress is uniform around the hole boundary. However, for the mixed field case, the final optimised shape is approximately rectangular with sharp corners and curved sides. Here, the absolute magnitude of the tangential stress has been rendered piecewise constant. The optimal shapes are presented in a tabular form that allows them to be used readily by designers. In a key numerical result, which has not been identified previously, it was found that the optimal shapes eliminate stress interaction effects, with the stress concentration produced by the optimal holes for both the tensile and mixed field biaxial loading cases being identical to the corresponding single hole optimal.

The procedures developed and the results obtained during this work have contributed to an enhanced capability in AVD for determining and specifying optimal shapes for extending the fatigue life of reworked holes in RAAF aircraft structural components.

Authors

Witold Waldman
Air Vehicles Division

Witold Waldman completed a BEng (with distinction) in Aeronautical Engineering at the Royal Melbourne Institute of Technology in 1981. He commenced work in Structures Division at the Aeronautical Research Laboratory in 1982. He has published a number of papers and reports, and his experience has focussed on finite element stress analysis, structural mechanics, computational unsteady aerodynamics, structural dynamics testing, digital filtering, non-linear optimisation and spectral analysis. His recent work has been in the areas of structural shape optimisation and loadpath visualisation. He is currently a Science and Technology Officer, Level 6, in the Air Vehicles Division.

Dr Manfred Heller
Air Vehicles Division

Manfred Heller completed a BEng (Hons.) in Aeronautical Engineering at the University of New South Wales in 1981. He commenced work in Structures Division at the Aeronautical Research Laboratory in 1982. He was awarded a Department of Defence Postgraduate Cadetship in 1986, completing a PhD at Melbourne University in 1989. He has an extensive publication record focussing on the areas of stress analysis, fracture mechanics, fatigue life extension methodologies and experimental validation. Since 1992 he has led tasks that develop and evaluate techniques for extending the fatigue life of RAAF aircraft components and provide specialised structural mechanics support to the RAAF. He is currently Head, Structural Mechanics, in the Air Vehicles Division.

Dr Francis Rose
Platforms Sciences Laboratory

Francis Rose graduated with a BSc (Hons.) from Sydney University in 1971, and a PhD from Sheffield University, UK, in 1975. He was appointed as a Research Scientist at the Aeronautical Research Laboratory in 1976, and he is currently holding the position of Chief Scientist in Platforms Sciences Laboratory. He has made important research contributions in fracture mechanics, non-destructive evaluation and applied mathematics. He is the regional editor for the International Journal of Fracture and a member of the editorial board of Mechanics of Materials. He is also a Fellow of the Institute for Applied Mathematics and its Applications, UK, and a Fellow of the Institution of Engineers, Australia.

Contents

1. Introduction

Multiple interacting closely-spaced holes are a common feature in aircraft (e.g. F-111 wing pivot fitting) and other engineering structures, and they are often fatigue-prone locations because of the stress concentrations that they introduce. As a result, the analysis of the stress concentrations caused by interacting circular holes has been of particular interest (Ling, 1948; Heywood, 1952, 1969; Haddon, 1967; Christiansen, 1968). In many cases, the holes are circular in shape because of ease of manufacturing considerations, but other shapes such as ellipses have also been considered to try to reduce stress concentration effects. Ideally, designers would like to be able to minimise the resultant stress concentrations for interacting holes, and the associated problem of determining optimal hole shapes has important practical ramifications for maximising the fatigue life of aircraft components. As a result, the problem of determining optimal shapes for interacting holes has been the subject of considerable study.

Cherepanov (1974) studied two interacting holes in a biaxially loaded plate with uniform loads of the same sign and a constant internal uniform pressure p acting on the boundary of the holes. The concept that the tangential stress was constant around the boundary of an optimal hole was mentioned. Although an analytical solution was presented for what was considered at the time to be the case of closely-spaced holes, there was an error in the expression for the edge separation distance. This meant that in practice the holes were not at all closely spaced, so any stress interaction effects were in fact minimal. Vigdergauz (1976) studied plates with n interacting holes in a biaxially loaded plate with uniform loads, with each hole loaded by a uniform pressure p. Although example solutions of optimal hole contours were presented for $n = 2$, 3, 4 and 6 holes, the loading was greatly simplified and consisted only of the internal pressure p (no remote loading). Because the presence of remote loads is such a typical characteristic of aircraft structures, these solutions have highly restricted scope for any possible practical applications. A significant ancillary outcome of this work was a correction to the expression for the edge separation distance in the hole geometry equations provided previously in Cherepanov (1974).

Vigdergauz (1977) once again studied a biaxially loaded plate with uniform loads and n holes, with each hole internally loaded by a uniform pressure p. A proof was given that the tangential stress around an optimal hole contour is a minimum compared to the maximum obtained on any other hole contours, which supported the assumption that had been utilised earlier by Cherapanov (1974). Example optimal hole shapes loaded only by an internal pressure p were provided for $n = 3$ and 4, but for only one edge separation distance per case. Analytical expressions corresponding to the optimal hole shapes for $n = 3$ were given. Banichuk (1977) also studied plates with n holes, providing another proof that an equi-stressed boundary is optimal, but no hole shapes were provided. Vigdergauz (1982) considered the case of two interacting holes in a plate, aligned on a line perpendicular to the direction of the applied load, with the holes themselves also loaded by a constant pressure p. A procedure for obtaining an approximate numerical solution was described for this pair of holes, but this was valid only for quite large hole separations, where any interaction effects would be small. Some shapes and stress concentration factors as a function of the interaction distance were provided for the loading case where the internal pressure was the only

applied load. Vigdergauz (1988) again revisited the problem of n interacting holes in a plate, giving optimality conditions but no optimal shapes. His work indicated that the tangential stress around the optimal hole boundary is the same for all cases, i.e. 2 to n holes.

Notwithstanding all of the above activity to date, no paper gives the stress concentration factors and optimal shapes for biaxially loaded plates with two closely-spaced interacting holes for a range of interaction distances. To this end, the recently developed AVD gradientless shape optimisation procedure, which is based on the use of finite element analysis (FEA) in an iterative manner, appears to be ideally suited to the present problem, as it has previously been applied successfully to problems involving fillets and single holes.

For the case of two interacting holes, the general problem geometry and the corresponding notation are shown in Figure 1. Here, the large rectangular plate contains two centrally located holes of height h and width w. For circular holes of radius r we have that $h = w = 2r$. The plate is subjected to uniform biaxial remote stresses along the remote edges of S_1 in the x-direction and S_2 in the y-direction. The distance between the edges of the two holes is e and the width and height of the plate are $24h$ and $27h$, respectively, and have been chosen to be much greater than r.

In general, the local stress concentration factor K_t around the boundary of a stress concentrating structural feature is usually defined as

$$K_t = \frac{\sigma_{local}}{\sigma_{nominal}} \tag{1}$$

where σ_{local} is the value of the local stress at any given point on the boundary and $\sigma_{nominal}$ is some nominal applied stress. It is possible to determine a peak value of K_t for any given configuration of stress concentrator geometry and loading conditions.

When choosing suitable hole configurations, designers often rely on circular or elliptical hole profiles, for which the maximum stress concentration factors are provided for some standardised geometries and loading cases (see Pilkey, 1997). However, as compared to the optimal holes obtained in the present work, it is has been found that the performance of circular or elliptical holes is poor in terms of the associated peak value of K_t. Nevertheless, there have historically been a number of reasons why circular holes, in particular, have continued to be so common: (i) ease of visualisation, drawing and manufacture; (ii) there are very limited analytical solutions for interacting true optimal shapes, with these only available for restrictive geometric configurations and/or loading cases that were amenable to analysis (e.g. see Cherepanov, 1974, and Vigdergauz, 1982); and (iii) accurate numerical or experimental methods are needed to determine optimal hole profiles for realistic cases (however, unfortunately, no such transferable data exist). In relation to (iii), it appears that only recently have high-quality finite element (FE) based shape optimisation procedures become commonly available. The fact that the optimal hole profiles need to be reproduced accurately in order to deliver the full optimal K_t value is not considered to be a problem, as modern machining techniques can readily meet the precision requirements.

Optimal hole shapes are relevant at the design stage, as well as having applications in local shape reworking during service to remove cracks at previously non-optimal holes. For

example, the application of free-form shape optimisation (for holes and fillets) in a systematic and automated manner has been of particular recent interest in AVD in order to obtain the most benefit from local shape reworking. Examples of this work include Kaye and Heller (1997), Heller et al. (1999), Chen et al. (2000), Kaye and Heller (2000), Heller et al. (2000a, 2000b), Waldman et al. (2000), Burchill et al. (2002), and Heller et al. (2002a, 2002b). It is important to note, as will be discussed in subsequent sections, that an essential requirement for optimality is achievement of uniform tangential stress along that segment of the boundary that is being optimised (see Baud, 1934; Heywood, 1945; Neuber, 1972; Cherepanov, 1974; Banichuk, 1977; Schnack, 1979; Vigdergauz and Cherkayev, 1986; Mattheck and Burkhardt, 1990; Kaye and Heller, 1997; Waldman et al., 2001). In the context of reworking existing structural components, the procedure must be implemented in accordance with the constraint that reshaping must involve material removal. However, the procedure could equally well allow for material addition, which would be appropriate for shape optimisation at the design stage.

In this paper, accurate solutions are determined for the optimal hole shapes for two closely-spaced holes in a large biaxially loaded plate. Initially, in Section 2 the key features of optimal holes and notches are discussed, along with a description of a recently developed finite element based gradientless shape optimisation procedure, which is employed to obtain the optimal shapes. This is followed in Sections 3 and 4 with detailed stress concentration results for holes under two distinct biaxial loading cases, as well as the normalised coordinates for the optimal profiles. These two biaxial loading cases are termed tensile field when the remote principal stresses are of the same sign, and mixed field when they are of opposite sign. A range of interaction distances, e/h, is considered for both the tension and mixed field cases.

2. Shape optimisation method for holes and notches

2.1 General features of optimal holes and notches

It is clear that a key feature of the best iterative numerical shape optimisation methods is the determination of a boundary shape so that there is a constant, or near constant, distribution of tangential stress around the boundary. The existence of this feature has been shown experimentally by Baud (1934) and Heywood (1945), and numerically by Schnack (1979), Mattheck and Burkhardt (1990), Heller et al. (1999), Waldman et al. (2000), Waldman et al. (2002) and Heller et al. (2002a, 2002b), to be consistent with the aim of minimising the peak stresses. Typically, if geometry constraints are placed on the possible shape, then the optimal shape will result in tangential stresses that can only be rendered uniform along part of the boundary. This feature appears to have been postulated first by Neuber (1972), and has been used successfully in shape optimisation of fuel flow vent holes and stiffener runouts in the F-111 wing pivot fitting (Heller et al., 2001a, 2001b) to increase fatigue life by reducing the magnitude of stress concentrations. In such cases, there is usually a sharp corner in the optimal geometry at the end of the uniform stress region (but without stress singularity), after which the stress decays rapidly. It is noted that those analytical solutions that are available for optimal holes typically rely on special geometric or loading conditions in order to be able to obtain solutions where the tangential stress around the hole is rendered

constant or piecewise constant for the entire hole boundary (e.g. Cherepanov, 1974; Vigdergauz, 1982; Vigdergauz and Cherkayev, 1986; Cherkaev et al., 1998). For this reason, the practical applicability of such analytical solutions is judged to be effectively non-existent when it comes to their potential use in typical aircraft structures, particularly when the applied loading is complex.

2.2 Shape optimisation using gradientless finite element method

In recent work in AVD, a highly effective iterative 2D gradientless free-form shape optimisation algorithm has been developed and implemented using the standard PAFEC Level 8.5 FEA code (see Kaye and Heller, 1997; Heller et al., 1999; Heller et al., 2001a; Heller et al., 2001b; and Waldman et al., 2001). The PAFEC FEA code is invoked directly by an in-house developed Fortran program during each iteration, and it has been used for all the FEA computations described in this paper. The general approach that is followed here is based on an analogy with the growth behaviour of biological structures, where material is added at regions of high stress and/or removed where the stress is low, a concept that was first identified by Thompson (1917). This FE-based approach can achieve a free-form optimal shape that produces a constant boundary stress distribution. Apart from the present approach, shape optimisation (albeit of differing effectiveness) based on biological growth analogies has been utilised experimentally by Heywood (1945) and numerically by Mattheck and Burkhardt (1990). However, in contrast with the numerical work of Mattheck and Burkhardt (1990), the present approach is significantly simpler, both in terms of the approach taken for defining local material removal/addition on the free boundary, as well as in terms of the method used for remeshing between iterations in order to avoid mesh distortion. Additionally, a particular distinction is that the present work focuses on the more difficult aspect of constrained reworking, as opposed to the shape optimisation of initial designs that may be less constrained.

In the context of hole shape optimisation, the present gradientless method can be explained as follows. Consider Figure 2a, which shows a plate with a hole (stress concentrator) with a free boundary, Γ, on which there are a number of nodes $i = 1,\ldots,k$, under an arbitrary remote loading. For an arbitrarily shaped (non-optimised) hole, the tangential stress will generally vary around the boundary, as shown schematically in Figure 2b. Here, the tangential stress is defined to be the non-zero principal stress at the free boundary. For simplicity here, let us assume that all the boundary stresses are positive in sign. The amount of material to be added or removed at any point on the boundary is taken to be directly proportional to the difference between the local tangential stress and a suitable reference value (Heller et al., 1999). This process is then repeated iteratively until the boundary hoop stress is constant, or nearly constant, to within a prescribed tolerance. The amount to move any given node i on the boundary at each iteration (in the direction of the outward normal) is specified by the following equation

$$d_i = \left(\frac{|\sigma_i| - |\sigma_{th}|}{|\sigma_{th}|} \right) cs \qquad (2)$$

where a positive value of d_i indicates material addition, σ_i is the tangential stress at node i on the boundary, σ_{th} is a non-zero threshold boundary hoop stress, c is an arbitrary characteristic length such as the initial hole radius, and s is an arbitrary step-size scaling factor typically in the range of 0.001–0.05 (see Kaye and Heller, 1997; Heller et al., 1999; Heller et al., 2001a; Heller et al., 2001b; and Waldman et al., 2001). The parameters c and s remain fixed throughout the shape optimisation process.

In relation to the selection of the parameter σ_{th}, a number of interesting features become apparent. Here, the specific magnitude of the threshold stress will define the type of shape optimisation process: (i) if we select σ_{th} to be less than the maximum stress, but more than the minimum stress, material will be both added and removed at various locations around the boundary; (ii) if we select σ_{th} to be the same or greater than the maximum stress, only material removal will occur; and (iii) if we select σ_{th} to be the same or less than the minimum stress only material addition will occur. If we are reworking a stress concentrator in an existing component, we must use option (ii) or option (i) with a further constraint on boundary movements so that material is not added (i.e. $d_i \leq 0$). In practical problems where there are geometrical constraints restricting the possible shape, the optimal shape may have two or more constant stress regions. For some problems it may be desirable to separately optimise the peak stresses in two different regions, and this can be accomplished by choosing two different values of σ_{th} and hence optimising each region independently, albeit simultaneously. This approach was used in Heller et al. (2001b). It is also noted that, by the inclusion of absolute value signs in Eq. (2), the general algorithm also works well to minimise compressive peaks (if they exist).

The shape optimisation method described above is highly suitable for implementation with any standard FEA code that permits the movement of nodes after the completion of an analysis. For such an iterative procedure, a useful parameter that can be used to monitor solution convergence is the normalised range in K_t around the hole boundary. This can be written as

$$\Psi = \frac{K_t^{\max} - K_t^{\min}}{K_t^{\text{avg}}} \tag{3}$$

where $K_t^{\max}$, $K_t^{\min}$, and K_t^{avg} are the maximum, minimum, and average values of K_t around the hole boundary. Clearly, as Ψ approaches zero, the stress becomes more uniform around the boundary and the optimal hole shape is approached.

2.3 Procedure for local element remeshing and hole shape specification

In the present work, the implementation of the shape optimisation algorithm with the standard FEA code PAFEC was used, as has been the case in prior work. Using a valuable and convenient mesh generation feature named PAFBLOCKs, only the nodal movements at the stress concentrator boundary need to be specified. For two-dimensional FE analyses, the mesh generation blocks are usually four-sided subregions of the FE model consisting of a number of plate elements. Figure 3 shows two mesh generation blocks, which are labelled as

B1 and B2. Using two parameters, N_1 and N_2, each mesh generation block can be subdivided into a number of smaller elements in the spanwise and chordwise directions as shown in the diagram. The parameters N_1 and N_2 define how many elements are to be created within each mesh generation block, as well as the spacing of those elements. In order for proportionately sized internal elements to be created, only the locations of the corner nodes and the number of elements along the sides of the blocks need to be specified. The moving boundary during the shape optimisation is denoted by the grey line, while the edges of the elements within each mesh generation block are denoted by the dotted lines. For each mesh generation block, note that the edge of the block that lies opposite to the moving boundary remains fixed, and the fixed boundary is denoted by the thick solid black line in the diagram.

Within the PAFEC code, the edges of each mesh generation block are defined by two corner nodes and a midside node in such a way that these three nodes lie on a circular arc or a straight line segment. The former applies for the initial FE mesh consisting of a circular hole. These multiple circular arcs are used by PAFEC for the generation of intermediate nodes. At every iteration during the shape optimisation, the nodes on the free boundary that define the edges of each of the mesh generation blocks are completely free to move to any location in accordance with Eq. (2). The internal elements within each of the mesh generation blocks simply shrink or grow in proportion to this nodal movement, which helps to maintain mesh integrity by avoiding mesh distortion, something that often causes problems for other FE-based shape optimisation programs. To some extent, the selection of the number of segments to be used to subdivide and model the moving boundary is arbitrary. However, if there are not enough segments then this will be readily apparent in the solution stresses, which will not be uniform along the hole boundary as required for a true optimal solution.

Consider the case where there are n element corner nodes arbitrarily spaced along a typical side of a mesh generation block that consists of a straight edge. At the m^{th} iteration, the coordinates (x_j, y_j) of the j^{th} node are as shown in Figure 3. The predicted movement of the boundary node (x_1, y_1) is $d_1 = (\Delta x_1, \Delta y_1)$. Then the new coordinates of the n element corner nodes at iteration m+1 can be computed using

$$x_j^{m+1} = x_j^m + \Delta x_1^m \left(\frac{x_j^m - x_n^m}{x_1^m - x_n^m} \right) \tag{4}$$

$$y_j^{m+1} = y_j^m + \Delta y_1^m \left(\frac{y_j^m - y_n^m}{y_1^m - y_n^m} \right) \tag{5}$$

2.4 General modelling details

For the analysis of the example problems described in Section 3, there were two elements per mesh generation block along the moving boundary. However, in Section 4, because of the presence of sharp corners in the optimal shape for the mixed field case, only one element per mesh generation block was used along the moving boundary.

All of the FE analyses that are reported on here were undertaken using a Hewlett-Packard K260 Series 9000 computer. All of the FE meshes consisted of 8-noded quadrilateral isoparametric elements and linear elastic plane stress conditions were assumed, with Young's modulus $E = 73$ GPa and Poisson's ratio $\nu = 0.32$ (which are material constants that are typical of an aluminium alloy).

2.5 Loadpath visualisation

An important issue related to computational efficiency and the avoidance of mesh distortion during the course of the shape optimisation is the judicious choice of the initial hole shape. Here it is desirable to have an indication of what the eventual optimal shape will be, in order to guide mesh definition. In this context, based on some prior work, loadpath visualisation could be a useful tool. A novel procedure for computing and visualising 2D loadpath orientations and loadpaths, using FEA results, has recently been developed by Kelly and Elsley (1993, 1995) and Kelly and Tosh (1998). Kelly and Elsley defined a loadpath to be the trajectory taken within a structure by a unit quantity of applied load, beginning at a point of application and ending at an equilibrating reaction. They introduced the concept of a hypothetical force "stream tube", which is depicted in Figure 4. For any selected resolved force direction, depicted as the x-direction in Figure 4, there is no flow of load across the boundary of the force tube, and the loadpath is therefore bounded by lines along which there is no contribution to the force in the x-direction. Note that in Figure 4 the applied and reaction loads F_{xa} and F_{xb} are aligned with the x-direction, but an equivalent diagram can also be produced for the forces in the y-direction (or any other chosen direction).

In more recent work by Waldman et al. (1999, 2002b), simple explicit equations for the computation of the x-direction and y-direction loadpath orientations, α_x and α_y, at any point on the structure have been derived, and these are as follows:

$$\tan\alpha_x = \frac{\tau_{xy}}{\sigma_x} \tag{6}$$

$$\tan\alpha_y = \frac{\sigma_y}{\tau_{xy}} \tag{7}$$

where σ_x is the normal stress in the x-direction, σ_y is the normal stress in the y-direction, and τ_{xy} is the shearing stress. The above equations have been applied to computing loadpaths for unconstrained optimal and initial non-optimal single holes in plates under uniaxial and biaxial loads (Waldman et al., 1999, 2002b). Particular features of these optimal shapes for single holes were identified, namely the absence of loadpath recirculation regions in the plate. The loadpath visualisation methodology developed previously is used here to study loadpaths for the present case of two closely-spaced interacting holes. It is considered desirable to do so in order to assess the behaviour of loadpaths when multiple holes are involved, as this particular configuration has never been investigated in this manner.

3. Analysis of two closely-spaced holes – tensile field

3.1 Analysis of initial geometry

For the present numerical analyses, the remote biaxial stresses were both tensile with $S_1 = S_2$, and the hole radius was taken as $r = 20$ mm ($h = 40$ mm). Due to symmetry, only one quarter of the plate was modelled in the FEA. The FE mesh to be used in the shape optimisation consisted of 2024 elements and it is shown in Figure 5a. A more detailed view of the region around one of the holes is shown in Figure 5b, including the node numbering along the moving boundary and the distribution of mesh generation blocks used to define the hole boundary. The mesh generation blocks are denoted by the thicker black lines, while the mesh generation block edges that are fixed are denoted by the thickest black line. The K_t value around the hole boundary for this geometry and loading condition was defined as

$$K_t = \frac{\sigma_i}{S_2} \tag{8}$$

where σ_i is the value of the local tangential stress at node i on the hole boundary. For this case with an edge separation distance $e/h = 0.5$, the peak K_t for the initial geometry was 2.906 at the location $(x, y) = (0, -h/4)$. It should be noted that, for a single circular hole in an infinite plate under this loading, a constant value of $K_t = 2.0$ occurs around the entire hole boundary.

3.2 Shape optimisation analyses and results

For convenience, the shape optimisation was undertaken for the context of reworking, where only material removal is allowed. Thus, at each iteration, all nodal movements on the hole boundary were constrained such that $d_i \leq 0$. The constraint on these nodal movements was achieved by selecting the threshold stress used in Eq. (2) to be equal to the maximum tangential stress occurring at the nodes on the hole boundary at each iteration:

$$\sigma_{th} = \underset{i=1}{\overset{k}{\text{Max}}}(\sigma_i) \tag{9}$$

The characteristic length c was defined to be equal to the radius of the initial circular hole, while the step-size scaling factor was set to $s = 0.02$. The other constraint on the shape optimisation domain required that the minimum allowable distance between the holes be fixed, which for the ¼-symmetry FE model means that $y \leq -e/2$ for any point on the hole boundary.

A typical solution geometry is shown in Figure 6, and it was obtained after 374 iterations using an initial geometry consisting of two circular holes with edge separation distance $e/h = 0.5$. Note that the edge separation distance between the two optimal holes has been reduced to $e/h = 0.4568$ because of an increase in the height of the holes that results from material removal during the shape optimisation process (the width of the holes also increased, from an initial $h/w = 1.0$ to $h/w = 0.7182$). A comparison of the stress concentration

factor K_t around the hole boundary for the optimal shape and the corresponding circular hole with $e/h = 0.4568$ is presented in Figure 7. For the optimal shape, the K_t values at the nodes along the hole boundary have been reduced to an essentially constant level, and they lie within a range of 2.013 to 2.009 (the range being equivalent to 0.36% of S_2). This represents a reduction of 32.7% compared to the peak stress concentration value of $K_t = 2.990$ for the two interacting circular holes with $e/h = 0.4568$ (determined in a separate analysis). It is clear that the K_t value for the two-hole optimal approaches the K_t value for the single-hole optimal in an infinite plate for this biaxial loading case, which corresponds to a circular hole with $K_t = 2.0$.

Figure 8a shows a contour plot of the normalised bulk stress distribution around the initial circular hole, while Figure 8b shows the equivalent results for the optimal hole. Here, the normalised bulk stress $\hat{\kappa}$ is defined as

$$\hat{\kappa} = \frac{\kappa}{S_1 + S_2} \tag{10}$$

Here the 2D bulk stress κ (which is the same as the first stress invariant) is defined as

$$\kappa = \sigma_x + \sigma_y = \sigma_{11} + \sigma_{22} \tag{11}$$

where σ_{11} and σ_{22} are the principal stresses.

A comparison of Figures 8a and 8b reveals a large difference in the two normalised bulk stress distributions, with the bulk stress distribution for the optimal solution demonstrating an important feature. Within a tolerance ranging between -0.5% and +1.4% of the remote normalised bulk stress, the normalised bulk stress contours shown in Figure 8b are essentially uniform for the entire plate, being almost identical (i.e. only slightly higher) to those for the plate without any holes. (A separate FEA was undertaken for the no-hole case.) This is the requirement, as proposed by Bjorkman and Richards (1976), for an optimal single hole to be regarded as being harmonic for loading conditions where $S_1S_2 > 0$, whereupon the introduction of the optimal hole must leave the original stress field in the absence of the hole everywhere unchanged. The fact that this property of being harmonic also applies to a case with two interacting holes has never previously been explicitly identified. It is worth noting that the optimal shape looks similar to the deloid given by Bjorkman and Richards (1979) for the single hole configuration; however, in that particular case, the deloid was computed for a quite different load case involving a non-uniform stress field with linear gradients. It is clear that the abovementioned requirement for optimal harmonic hole shapes will only be exactly satisfied for infinite plates. This is because finite-width plates will always have a higher average bulk stress resulting from the stiffness loss due to the presence of the hole.

Using the present method, optimal shapes and their associated K_t values were then determined for three additional edge separation distances, namely $e/h = 0.2101$, 0.9756 and 1.4815. For these cases, the edge separation distances for the initial circular holes were $e/h = 0.25$, 1.0 and 1.5, respectively. The K_t results for the complete set of four optimal shapes are given in Table 1, together with the K_t values that were calculated for the equivalent non-optimal circular holes. The results for two circular holes for a number of additional values of

e/h are also tabulated. It should be noted that the peak K_t for the circular holes always occurred at the location corresponding to node 60 in Figure 5b, which lies on the symmetry line $x = 0$. From the results, it is evident that the optimal K_t values represent a large reduction as compared to the corresponding K_t values for non-optimal interacting circular holes, with the optimal K_t values lying in the range 2.015 to 2.010. These values are equal to the average of the K_t values at the nodes around the boundary of the hole, and the variation was less than 0.2% of each average value.

Table 1 also presents a comparison of the K_t values that were determined using an analytical solution for the stress in an infinite plate with two equal circular holes (Ling, 1948) and the present FEA computations for various e/h values. The present FEA results are all in excellent agreement with those determined by Ling (1948), although in each case the K_t value from the FEA is slightly higher than the analytical, but never by more than 0.79%. It is considered that these slight differences are due to the influence of the finite plate width on the FEA.

Figure 9 shows a plot of K_t versus e/h for the complete set of results for the optimal holes and the non-optimal circular holes. The optimal K_t values are essentially equal to 2 (to within 0.75%), with the slight increase above the value of 2 being due to the plate finite-width effects, which appear to increase a little as the edge separation distance is decreased. Originally, a plate one-third the size of the one shown in Figure 5 was used, but this produced a K_t value that was approximately 5% greater than 2, so the use of the larger plate was settled on.

Hence, the key result obtained here is that optimal shapes that ***eliminate stress interaction effects*** between two closely-spaced interacting holes have been determined numerically. This work has led to the unexpected finding that the peak K_t for two interacting optimal holes is identical to that for the corresponding optimal shape for a single hole. This is an important feature, which does not appear to have been previously noted anywhere in the available literature. For illustrative purposes, the optimal shapes determined in the present work are plotted in Figure 10, where it can be seen that, as the edge separation distance decreases, the shape of the two separate optimal holes approaches that of a single circular hole circumscribing them both. For the benefit of transferability to designers, the normalised coordinates for the family of optimal shapes are given in Table 2. Prior work by Waldman et al. (2000) has shown that a compact function cannot represent such optimal shapes accurately, and that designers should instead use cubic splines to interpolate these coordinates.

3.3 Comparison with analytical solution

It is noted that Cherepanov (1974) gives optimal solutions for plates containing two interacting holes, where the exterior of the two holes in the $Z = (x, y)$ plane is mapped conformally onto the exterior of two slits lying along the real axis of the complex $\zeta = \xi + i\eta$ plane. These two holes are aligned horizontally along the x-axis, which is perpendicular to the layout shown in Figure 1. In the general formulation for the symmetric case under consideration here, the width of each slit was set to unity and the two slits were assumed to lie within the bounds $1 < \xi < 2$ and $-2 < \xi < -1$. Under the conformal mapping, $\xi = \pm 1$ corresponds to the locations of the hole edges that are closest to the axis of symmetry, while

$\xi = \pm 2$ corresponds to the locations of the hole edges that are furthest from the axis of symmetry.

However, there is an error in the expression for x_B in Eq. 3.17 in Cherepanov (1974), which was discovered and subsequently corrected by Vigdergauz (1976). The complete and corrected equation for the hole shape is given below, where $e = 2x_B$ is the interaction (edge separation) distance between the two holes, p is a constant applied normal stress around the edge of each hole, and a homogeneous field of constant stress acts at infinity, where $\sigma_x = \sigma_x^\infty$ and $\sigma_y = \sigma_y^\infty$.

$$
\begin{aligned}
x &= x_B + \frac{1}{2}c_1\left(1-\frac{b}{a}\right)(\xi - 1) \\
y &= \pm\left\{-\frac{1}{2}c_1\left(1+\frac{b}{a}\right)\left(2E(\varphi,60^\circ) + \frac{1}{2}d_2 F(\varphi,60^\circ) - \frac{1}{\xi}\sqrt{(4-\xi^2)(\xi^2-1)}\right)\right\} \\
x_B &= c_1\left(d_1 + (d_1 - 1)\frac{b}{a}\right) \\
d_1 &= \frac{1}{2} + E(90^\circ,30^\circ) - F(90^\circ,30^\circ)\left(1+\frac{d_2}{4}\right) \\
d_2 &= -\frac{4E(90^\circ,60^\circ)}{F(90^\circ,60^\circ)} \\
\frac{b}{a} &= \frac{\sigma_x^\infty - \sigma_y^\infty}{\sigma_x^\infty + \sigma_y^\infty - 2p}, \quad \left|\frac{b}{a}\right| < 1 \\
\varphi &= \arcsin\left(\frac{2\sqrt{\xi^2-1}}{\xi\sqrt{3}}\right), \quad 1 < \xi < 2
\end{aligned}
\tag{12}
$$

Here the functions $F(\varphi,\alpha)$ and $E(\varphi,\alpha)$ are the elliptic integrals of the first and second kinds, respectively. The constant c_1, which gives the scale in the physical x-y plane, is considered to be real and positive, and remains undetermined by the formulation of the problem.

For the particular problem being considered here, we have $p = 0$. The edge separation distance is simply $e = 2x\big|_{\xi=1} = 2x_B$ and the height of the hole is $h = x\big|_{\xi=2} - x\big|_{\xi=1}$. This leads to the following expression for the edge separation distance e/h:

$$
\frac{e}{h} = \frac{4\left(d_1 + (d_1 - 1)\frac{b}{a}\right)}{1-\frac{b}{a}} \tag{13}
$$

where d_1 is a constant and has been calculated to be equal to 1.22840. From Eqs. (12) and (13), it is evident that both the optimal hole shape and the edge separation distance are solely functions of one parameter, b/a. Consequently, the key point here is that there is no explicit way to determine the optimal hole shape for a specified edge separation parameter e/h and load parameter b/a for a given practical problem, a factor that significantly limits the usefulness of the solution.

In Cherepanov (1974), the edge separation distance that was depicted for some of the optimal holes was small relative to the height of each hole. However, after applying the correction to the expression for x_B, it turns out that the edge separation distance between the holes is actually relatively large. This can readily be seen in Figure 11, where we consider a range of load cases S_2/S_1, with the values of e/h ranging from a high of 4.91 to a low of 2.15. Thus, based on the behaviour of the K_t for two interacting circular holes presented in Figure 9, any interaction effects are expected to be small for the biaxial loading cases that were considered by Cherepanov (1974), as the values of e/h that were used there were all greater than 2. We note here that the optimal shape for a single hole in a tensile biaxial stress field is an ellipse, whose aspect ratio h/w is equal to the biaxial load ratio S_2/S_1, producing a uniform stress distribution around the edge of the hole (Durelli and Murray, 1943). The hole shapes as determined by Cherepanov (1974) are in fact approximately elliptical, with their aspect ratios h/w almost equal to the biaxial load ratio S_2/S_1, as would be expected for pairs of holes for which the edge separation distance was large enough for any interaction effects to be negligible (i.e. as for a single optimal hole). Hence, it turns out that Cherepanov's solution is for holes that do not interact to any appreciable degree.

3.4 Comparison of loadpath distributions

Resolved x- and y-direction loadpaths for the initial and the optimal configurations were determined, and are given in Figure 12. For the initial case of the circular hole, depicted in Figures 12a and 12b, we see that compaction of the resolved x- and y-direction loadpaths occurs at the two peak stress locations, respectively. Although it was initially expected to be present, recirculation is not apparent in any of these loadpath plots. This is believed to result from the fact that the nominal and optimal shapes are relatively similar. It is also possible that a significantly more refined mesh would be needed to enable finer details to be observed. In prior work, Waldman et al. (1999) found that recirculation was a notable feature of non-optimal geometries. However, in that work, there was a significant shape difference between the initial and the optimal holes. For the present investigation, the plotted loadpaths show no clear distinguishing features between the initial and the optimal shapes.

4. Analysis of two closely-spaced holes – mixed field

4.1 Analysis of initial geometry

For this particular analysis, the biaxial remote stresses along the plate edges were taken as $S_1 = -½S_2$ (i.e. a mixed field with remote stresses of opposite sign and different magnitude), and the initial interaction distance was taken as $e/h = 0.5$. Once again, due to symmetry only

one-quarter of the plate was modelled in the FEA, and 2024 elements were used to define the mesh. The FE mesh for the plate with the initial circular hole is shown in Figure 13a, where the mesh refinement in the lower right-hand corner was required because of the high applied shear stress in that region (since the magnitude of S_1 is of the same order as S_2). The K_t value at the nodes around the hole boundary for this geometry and loading condition was defined as

$$K_t = \frac{\sigma_i}{S_2} \tag{14}$$

where S_2 is the dominant load component, and σ_i is the value of the local tangential stress at node i on the hole boundary. The peak K_t value for the initial geometry was equal to 3.132 at the location $(x, y) = (0.4985h, -0.7892h)$ on the hole boundary. This compares with a peak value of $K_t = 3.5$ for the case of a similarly loaded infinite plate containing a single circular hole, so it is apparent that a small degree of stress alleviation has resulted from having two circular holes in close proximity to each other because of shielding effects.

4.2 Shape optimisation results and discussion

The shape optimisation parameters were taken as $c = 20$ mm and $s = 0.02$. For these iterations, in order to minimise both the tensile and the compressive peak (which would be desirable in the case of fully reversed cyclic plate loading), the following value was taken for the stress threshold in Eq. (2):

$$\sigma_{th} = \frac{1}{k}\sum_{i=1}^{k} |\sigma_i| \tag{15}$$

Here the stress threshold σ_{th} is equal to the average value of the absolute stress around the hole boundary. This is useful for computational robustness in situations where overshooting of the true optimal solution is identified, as it allows material to be added as well as removed during the course of the shape optimisation. The fact that the final shape may encroach on the initial one is something that is allowable when carrying out shape optimisation for an initial design. However, in the event that a requirement exists for the optimal shape to lie outside some specified hole shape (such as when reworking only was allowed), then it would be necessary to start from a larger initial hole shape.

The final optimised finite element mesh after 341 iterations is shown in Figure 13b, and an enlarged view of the final solution geometry is shown in Figure 13c. It can be seen that the optimal shape has sharp corners and is approximately rectangular but with curved sides, with a height-to-width ratio $h/w = 1.3288$. As expected, and fully in accordance with Eq. (15), material addition as well as material removal has taken place around the hole boundary. This is evident when comparing Figures 13a and 13b, as most of the near-vertical side of the rectangle-like optimal shape has moved in leftwards towards the y-axis relative to the initial circular shape. The edge separation distance has also been reduced from an initial $e/h = 0.5$ to $e/h = 0.3224$ during the shape optimisation. A comparison of the stress distribution around the hole boundary for two interacting circular holes with $e/h = 0.3224$

and the optimal hole shapes is given in Figure 14. It can be seen that the absolute value of the stress concentration along the optimal hole boundary has been reduced to what is an essentially piecewise-constant level of $K_t = 1.9156$. As compared to the peak K_t value of 3.1195 for two interacting circular holes with $e/h = 0.3224$, the level of stress concentration has been reduced by 38.6%, which is an excellent improvement.

The above result has a number of key similarities to that of optimal ***single holes*** in an infinite plate under mixed loading where $S_1S_2 < 0$, for which Vigdergauz and Cherkayev (1986) have determined K_t values using a semi-analytical method. However, they did not present any calculated optimal hole shapes. They noted that the hole shapes are almost rectangular, having curved sides with corners of a definite included angle, with the ratio of the sides and the included angles being dependent on the applied loading. They also noted that: (i) a required condition for optimality was that the absolute magnitude of the tangential stress around the optimal hole boundary should be constant, with there being a discontinuous sign change in the stress at the corner points without any singularities; and (ii) the lack of any stress singularities is possible because of the corresponding discontinuous change in the local unit tangent vector at the corners. These characteristic geometric features of the optimal shapes and associated stress conditions have also been identified in the present work for two interacting holes in a plate under mixed loading, including the presence of sharp corners and the absence of corner singularities. These results are typical of optimal shapes obtained for mixed field loadings such as the one considered here, or for cases where geometric constraints are active (e.g. optimal fillets such as those considered by Waldman et al., 2001, and constrained holes such as those considered by Kaye and Heller, 1997).

For comparison purposes, in Figure 15 the predictions of peak K_t for a single optimal hole given by Vigdergauz and Cherkayev (1986) are plotted for various values of the biaxial load ratio, $-S_1/S_2$. Here they are compared to some other available solutions, including the present two-hole optimal solution of $K_t = \pm 1.92$ obtained for $-S_1/S_2 = 0.5$. A single-hole optimal solution of $K_t = \pm 2.84$ obtained for $-S_1/S_2 = 1.0$ using the present method is also shown. As can be seen, this result is very close to the approximate numerical solution of $K_t = \pm 2.73$ obtained by Vigdergauz and Cherkayev (1986). A key point to note here is that the optimal two-hole result is very similar to that for the case of a single optimal hole, indicating that the interaction effects between the two holes are negligible, a result that has not previously been available. The kink that is located near $-S_1/S_2 = 0.3$ on the curve corresponding to the single-hole optimal shape appears to indicate that there is a typographical error in the data published in Vigdergauz and Cherkayev (1986). Judging by the overall trend exhibited by the data, it would appear that the point corresponding to the value $-S_1/S_2 = 0.311$ and $K_t = 1.62$ is the one that is in error. For further comparison, two additional published results are given for the biaxial load ratio case $-S_1/S_2 = 1$ for similar but sub-optimal holes: Pilkey (1997) gives $K_t = 3.2$ for a single square hole (with rounded corners), and Durelli and Rajaiah (1979) give $K_t = 3.0$ for a single double-barrel quasi-square-shaped hole (also with rounded corners). As expected, both of these values are somewhat higher than the optimal value of $K_t = 2.73$ given by Vigdergauz and Cherkayev (1986).

For the mixed field case with two holes and a biaxial load ratio of $-S_1/S_2 = 0.5$, a number of different configurations were optimised to produce optimal holes for a variety of edge separation distances, e/h. Figure 16 shows a plot of K_t versus e/h for the optimal holes as well as the non-optimal circular holes. The K_t values for the optimal holes are reduced by

more than 35% compared to the equivalent circular holes, which is a very significant reduction. Furthermore, the optimal holes produce an essentially constant K_t that is independent of e/h for the range of interaction distances that were analysed, while the results for the circular holes show a small increase in K_t with increasing e/h. For the benefit of transferability to designers, the normalised coordinates for the family of optimal shapes are given in Table 3.

Figure 17 shows normalised bulk stress distributions (see Eq. (10)) for the initial circular hole as well as the final optimal hole. Inspection of Figures 17a and 17b, corresponding to the initial and the optimal solutions, respectively, reveals that there is a significant difference in the bulk stress distributions. Note that the peak values of normalised bulk stress are significantly reduced for the optimal case. However, unlike the case involving the biaxial tensile field loading for which $S_1S_2 > 0$, the bulk stress distribution is not uniform for the optimal shape for the mixed field loading for which $S_1S_2 < 0$, and hence the hole is not a harmonic hole. A hole is regarded as being harmonic if the bulk stress distribution in the plate without a hole present is unaffected by the inclusion of the hole (Bjorkman and Richards, 1976). Leading on from this, it was initially envisaged that, for the mixed field loading for which $S_1S_2 < 0$, the difference in the direct stresses $(\sigma_x - \sigma_y)$ throughout the plate might be unaffected by the presence of the optimal hole, leading to a new class of harmonic holes. However, it was found that this was not the case. Hence, it appears that it is doubtful that any further work is required to extend the concept of optimal harmonic holes to the mixed loading case. However, the present work confirms numerically that, as far as optimality is concerned, the essential requirement is piecewise uniformity of the tangential stress along the edge of the hole boundary.

4.3 Comparison of loadpath distributions

Resolved x- and y-direction loadpaths for the initial and the optimal configurations were determined, and are shown in Figure 18. For the case of the initial circular hole, Figure 18a reveals that compaction of the resolved x-direction loadpaths occurs at the two locations of peak compressive stress at the top and bottom of the hole, and a strong recirculation region is evident in the peak tension stress region on the right-hand side of the hole. The reverse of this behaviour is evident for the resolved y-direction loadpaths in Figure 18b. Convérsely, for the optimal shape, Figure 18c shows no recirculation in the x-direction loadpaths, while recirculation is apparent above and below the hole for the y-direction loadpaths, and compaction of the loadpaths is quite evident in both cases. Comparing Figures 18a and 18b to Figures 18c and 18d, the recirculation regions are significantly less pronounced for the optimal shape as compared to the initial circular shape. This is consistent with the findings by Waldman et al. (1999) in prior work for single-hole geometries. It is believed that the recirculation that is evident for this optimal shape results from the fact that sharp corners are present, which produce a rapid change in sign of the local stress field that may act like a boundary for the loadpaths.

5. Conclusion

In this report, accurate profiles of free-form optimal shapes and their associated stress concentration factors have been presented for large plates containing two closely-spaced interacting holes. Two distinct biaxial loading cases and a range of hole interaction distances have been investigated. In a key unexpected result, which has not previously been identified, it has been discovered that the peak stress associated with the optimal holes is independent of the interaction distance, and that the peak stress is the same as that for an optimal single hole. Overall, it has been demonstrated numerically that the nature of the distribution of tangential stress around the optimal hole boundaries depends critically on the sign of the product of the remote biaxial loads S_1 and S_2. For the tensile biaxial loading cases where $S_1S_2 > 0$, the tangential hoop stress is constant around the hole boundary. For the mixed field biaxial loading cases where $S_1S_2 < 0$, the absolute value of the tangential hoop stress is piecewise constant around the hole boundary. This characteristic behaviour for the mixed biaxial loading case was first identified by Vigdergauz and Cherkayev (1986). Compared to interacting closely-spaced circular holes, which are a common feature in aircraft structures producing significant stress concentrations that often lead to premature fatigue cracking, ***the optimal hole shapes provide for very large reductions in peak stress (typically greater than 30%)***, which results in a substantial increase in fatigue life.

The free-form optimal shapes are presented in a tabular form, which allows them to be used readily by designers. For the tensile biaxial loading case, the optimal shape is non-circular, and meets the definition for a harmonic hole (i.e. the bulk stress field in the loaded plate without a hole is unchanged by the inclusion of the optimal hole), which has never been identified in any prior work. For the mixed field biaxial loading case, the final optimised shape is approximately rectangular but with curved sides, and with sharp corners. When coupled with the discontinuous change in the local unit tangent vector at the corners, the discontinuous nature of the tangential stress either side of the corners does not produce any corner stress singularity (Vigdergauz and Cherkayev, 1986).

Loadpath visualisations for the tensile biaxial field case, where $S_1S_2 > 0$, found that no loadpath recirculation regions were present for either the circular or the optimal hole cases. This possibly occurred because the circular and optimal shapes could be considered as being relatively similar to each other. For the mixed field biaxial loading case, where $S_1S_2 < 0$, it was found that recirculation was significantly less pronounced for the optimal shapes as compared to the initial shape, and this is consistent with prior work for unconstrained single-hole geometries. It is believed that the existence of a recirculation region for the optimal hole shapes for $S_1S_2 < 0$ results from the presence of sharp corners, which produce a rapid change of sign in the local stress field that may act like a boundary for the loadpaths.

The procedures that were developed and the results obtained during this work have contributed to an enhanced capability in AVD for specifying optimal shapes for extending the fatigue life of reworked holes in RAAF aircraft structural components.

References

Banichuk NV, 1977. Optimality conditions in the problem of seeking the hole shapes in elastic bodies. Journal of Applied Mathematics and Mechanics, Vol. 41, No. 5, pp. 946–951 (English translation of Russian Prik. Matem. Mekhan., Vol. 41, No. 5, 1977, pp. 920–925).

Baud RV, 1934. Fillet profiles for constant stress. Product Engineering, April, pp. 133–134.

Bjorkman Jr. GS, Richards Jr. R, 1976. Harmonic holes – an inverse problem in elasticity. Journal of Applied Mechanics, Vol. 43, No. 3, September, pp. 414–418.

Bjorkman Jr. GS, Richards Jr. R, 1979. Harmonic holes for nonconstant fields. Journal of Applied Mechanics, Vol. 46, pp. 573–576.

Burchill M, McDonald M, Heller M, Watters KC, 2002. Shape optimisation of fatigue prone holes in the wing pivot fitting of the RAAF's F-111 aircraft. Applied Mechanics: Progress and Applications. Editors L Zhang, L Tong, J Gal. Proceedings of the Third Australasian Congress on Applied Mechanics, 20–22 February, Sydney, Australia, pp. 129–134.

Chen GX, Wang CH, Heller M, 2000. Optimisation of stop holes. Proceedings of the Australian Fracture Group Inc Structural Integrity and Fracture Symposium 2000, 29–30 June, University of Technology, Sydney, Australia.

Cherepanov GP, 1974. Inverse problems of the plane theory of elasticity. Journal of Applied Mathematics and Mechanics, Vol. 38, No. 6, pp. 915–930 (English translation of Russian Prik. Matem. Mekhan., Vol. 38, No. 6, 1974, pp. 963–979). See correction to Eq. 3.17 in Vigdergauz, 1976.

Cherkaev AV, Grabovsky Y, Movchan AB, Serkov SK, 1998. The cavity of the optimal shape under the shear stresses. International Journal of Solids and Structures, Vol. 35, No. 33, pp. 4391–4410.

Christiansen S, 1968. Numerical determination of stresses in a finite or infinite plate with several holes of arbitrary form. Z. angew. Math. u. Mech., Vol. 48, pp. T131–T134.

Durelli AJ, Murray WM, 1943. Stress distribution around an elliptical discontinuity in any two-dimensional, uniform and axial, system of combined stress. Proc. Soc. for Experimental Stress Analysis, Vol. 1, No. 1, pp. 19–31.

Durelli AJ, Rajaiah K, 1979. Quasi-square hole with optimum shape in an infinite plate subjected to in-plane loading. Report No. 49, School of Engineering, Oakland University, Rochester, Michigan 48063, USA.

Haddon RAW, 1967. Stresses in an infinite plate with two unequal circular holes. Quarterly Journal of Mechanics and Applied Mathematics, Vol. 20, pp. 277–291.

Heller M, Kaye R, Rose LRF, 1999. A gradientless procedure for shape optimisation. Journal of Strain Analysis, Vol. 34, No. 5, pp. 323–336.

Heller M, McDonald M, Burchill M, Watters KC, 2001a. Shape optimisation of critical stiffener runouts in the F-111 wing pivot fitting. DSTO-TR-1119, Defence Science and Technology Organisation, Department of Defence, Australia, April.

Heller M, Burchill M, McDonald M, Watters KC, 2001b. Shape optimisation of critical fuel flow vent holes in the F-111 wing pivot fitting. DSTO-TR-1120, Defence Science and Technology Organisation, Department of Defence, Australia, April.

Heller M, McDonald M, Burchill M, Watters KC, 2002a. F-111 airframe life extension through rework shape optimisation of critical features in the wing pivot fitting. 6th Joint FAA/DoD/NASA Aging Aircraft Conference, September 16–19, San Francisco, USA.

Heller M, McDonald M, Burchill M, Watters KC, 2002b. Shape optimization of critical stiffener runouts for F-111 airframe life extension. Fatigue & Fracture of Engineering Materials & Structures, Vol. 25, Issue 2, February, pp. 151–172.

Heywood RB, 1945. Photo-Elasticity and Design Problems: Part II. Aircraft Engineering, Vol. 17, August, pp. 226–228.

Heywood RB, 1952. Designing by photoelasticity. Chapman & Hall Ltd, London, England.

Heywood RB, 1969. Photoelasticity for designers. Pergamon Press, Oxford, England.

Kaye R, Heller M, 1997. Structural shape optimisation by iterative finite element solution. DSTO-RR-0105, Defence Science and Technology Organisation, Department of Defence, Australia, June.

Kaye R, Heller M, 2000. Investigation of shape optimisation for the design of life extension options for an F/A-18 airframe FS 470 Bulkhead. Journal of Strain Analysis, Vol. 35, No. 6, pp. 493–505.

Kelly DW, Elsley M, 1993. A procedure for determining loadpaths in elastic continua. Cooperative Research Centre for Aerospace Structures Ltd, Report CRC-AS EP 93500.

Kelly DW, Elsley M, 1995. A procedure for determining load paths in elastic continua. Engineering Computations, Vol. 12, pp. 415–424.

Kelly DW, Tosh MW, 1998. Load paths and stress trajectories in elasticity. Cooperative Research Centre for Advanced Composite Structures Ltd, Report CRC-ACS EP 97022.

Ling CB, 1948. On the stresses in a plate containing two circular holes. Journal of Applied Physics, Vol. 19, January, pp. 77–82.

Mattheck C, Burkhardt S, 1990. A new method of structural shape optimisation based on biological growth. International Journal of Fatigue, Vol. 12, No. 3, pp. 185–190.

Pilkey DW, 1997. Peterson's stress concentration factors, 2nd edition. John Wiley & Sons, Inc.

Neuber H, 1972. Zur Optimirung der Spannungskonzentration. Continuum Mechanics and Related Problems of Analysis. Nauka Publishing House, Moscow, pp. 375–380.

Schnack E, 1979. An optimisation procedure for stress concentrations by the finite element technique. International Journal for Numerical Methods in Engineering, Vol. 14, pp. 115–124.

Thompson DW, 1917. On growth and form. Cambridge University Press, London (also abridged edition. Bonner JT (Ed.), Cambridge University Press, London, 1961).

Vigdergauz SB, 1976. Integral equation of the inverse problem of the plane theory of elasticity. Journal of Applied Mathematics and Mechanics, Vol. 40, No. 3, pp. 518–522 (English translation of Russian Prik. Matem. Mekhan., Vol. 40, No. 3, 1976, pp. 566–569). Includes correction to Eq. 3.17 in Cherepanov, 1974.

Vigdergauz SB, 1977. On a case of the inverse problem of two-dimensional theory of elasticity. Journal of Applied Mathematics and Mechanics, Vol. 41, No. 5, pp. 927–933, (English translation of Russian Prik. Matem. Mekhan., Vol. 41, No. 5, 1977, pp. 902–908).

Vigdergauz SB, 1982. Equal strength hole in a half-plane. Mechanics of Solids, Vol. 17, No. 1, pp. 87–91 (English translation of Russian Ivz. AN SSSR, Mekhanika Tverdogo Tela, Vol. 17, No. 1, 1982, pp. 94–98).

Vigdergauz SB, 1983. Inverse problem of three-dimensional elasticity. Mechanics of Solids, Vol. 18, No. 2, pp. 83–86 (English translation of Russian Ivz. AN SSSR, Mekhanika Tverdogo Tela, Vol. 18, No. 2, 1983, pp. 90–93).

Vigdergauz SB, 1986. Effective elastic parameters of a plate with a regular system of equal-strength holes. Mechanics of Solids, Vol. 21, No. 2, pp. 165–169 (English translation of Russian Ivz. AN SSSR, Mekhanika Tverdogo Tela, Vol. 21, No. 2, 1986, pp. 162–166).

Vigdergauz SB, Cherkayev AV, 1986. A hole in plate, optimal for its biaxial extension-compression. Journal of Applied Mathematics and Mechanics, Vol. 50, No. 3, pp. 401–404 (English translation of Russian Prik. Matem. Mekhan., Vol. 50, No. 3, 1986, pp. 401–404).

Vigdergauz SB, 1988. Stressed state of an elastic plane with constant-stress holes. Mechanics of Solids, Vol. 23, No.3, pp. 96–99 (English translation of Ivz. AN SSSR, Mekhanika Tverdogo Tela, Vol. 23, No. 3, 1988, pp. 101–104).

Waldman W, Heller M, Rose LRF, 1999. Advances in structural loadflow visualisation and applications to optimal shapes. DSTO-RR-0166, Defence Science and Technology Organisation, Department of Defence, Australia, October.

Waldman W, Heller M, Chen GX, 2001. Optimal free-form shapes for shoulder fillets in flat plates under tension and bending. International Journal of Fatigue, Vol. 23, pp. 509–523.

Waldman W, Heller M, McDonald M, Chen GX, 2002a. Developments in rework shape optimisation for life extension of aging airframes. Third Australasian Congress on Applied Mechanics, ACAM 2002, 20–22 February, University of Sydney, Sydney, Australia, pp. 695–702.

Waldman W, Heller M, Kaye R, Rose LRF, 2002b. Advances in structural loadflow visualisation. Engineering Computations, Vol. 19, No. 3, pp. 305–326.

Table 1: K_t values for two interacting holes of circular and optimal shape in a large plate under remote biaxial loading $S_1 = S_2$ for various e/h values.

e/h	K_t for circular holes			K_t for optimal holes from present FEA
	Ling (1948)	Present FEA	Difference FEA vs Ling	
0.2101	–	3.955	–	2.015
0.2500	–	3.682	–	–
0.3500	–	3.259	–	–
0.4568	–	2.990	–	2.011
0.5000	2.887	2.906	+0.65%	–
0.6000	–	2.755	–	–
0.7500	–	2.595	–	–
0.9756	–	2.437	–	2.010
1.0000	2.411	2.426	+0.62%	–
1.2500	–	2.322	–	–
1.4815	–	2.258	–	2.010
1.5000	–	2.254	–	–
2.0000	2.155	2.172	+0.79%	–
4.0000	2.049	–	–	–
7.0000	2.018	–	–	–
∞	2.000	–	–	–

Table 2: Coordinates of optimal shapes for two interacting holes in a large plate under remote biaxial loading $S_1 = S_2$ *for various* e/h *values.*

$S_1 = S_2$							
$e/h = 0.2101$ $K_t = 2.0150$ $h/w = 0.6015$		$e/h = 0.4568$ $K_t = 2.0110$ $h/w = 0.7182$		$e/h = 0.9756$ $K_t = 2.0100$ $h/w = 0.8601$		$e/h = 1.4815$ $K_t = 2.0100$ $h/w = 0.9139$	
x/h	y/h	x/h	y/h	x/h	y/h	x/h	y/h
0.0000	0.1050	0.0000	0.2284	0.0000	0.4878	0.0000	0.7407
0.0555	0.1050	0.0484	0.2286	0.0428	0.4888	0.0412	0.7420
0.1110	0.1050	0.0969	0.2292	0.0854	0.4918	0.0822	0.7458
0.1665	0.1050	0.1453	0.2304	0.1279	0.4968	0.1230	0.7521
0.2220	0.1050	0.1937	0.2322	0.1700	0.5040	0.1632	0.7610
0.2775	0.1050	0.2421	0.2349	0.2117	0.5135	0.2028	0.7726
0.3330	0.1050	0.2904	0.2387	0.2528	0.5254	0.2414	0.7868
0.3885	0.1051	0.3385	0.2442	0.2930	0.5401	0.2790	0.8038
0.4440	0.1054	0.3864	0.2518	0.3320	0.5575	0.3152	0.8235
0.4995	0.1059	0.4337	0.2624	0.3696	0.5780	0.3498	0.8459
0.5550	0.1073	0.4799	0.2769	0.4053	0.6015	0.3824	0.8711
0.6104	0.1104	0.5242	0.2964	0.4386	0.6283	0.4128	0.8989
0.6654	0.1180	0.5656	0.3216	0.4693	0.6580	0.4407	0.9293
0.7185	0.1342	0.6025	0.3530	0.4968	0.6908	0.4658	0.9620
0.7649	0.1645	0.6337	0.3900	0.5209	0.7262	0.4878	0.9968
0.7981	0.2090	0.6586	0.4316	0.5411	0.7638	0.5066	1.0335
0.8184	0.2607	0.6770	0.4764	0.5573	0.8034	0.5219	1.0718
0.8288	0.3152	0.6891	0.5233	0.5694	0.8444	0.5337	1.1113
0.8313	0.3706	0.6953	0.5714	0.5774	0.8864	0.5418	1.1517
0.8276	0.4260	0.6962	0.6198	0.5813	0.9290	0.5463	1.1926
0.8184	0.4808	0.6922	0.6681	0.5812	0.9718	0.5471	1.2339
0.8046	0.5345	0.6837	0.7158	0.5771	1.0143	0.5444	1.2750
0.7863	0.5869	0.6709	0.7625	0.5693	1.0564	0.5381	1.3157
0.7641	0.6378	0.6543	0.8080	0.5579	1.0976	0.5283	1.3558
0.7382	0.6869	0.6340	0.8520	0.5431	1.1377	0.5153	1.3949
0.7089	0.7340	0.6104	0.8943	0.5250	1.1765	0.4991	1.4328
0.6763	0.7789	0.5837	0.9347	0.5039	1.2137	0.4799	1.4692
0.6407	0.8215	0.5541	0.9731	0.4800	1.2491	0.4579	1.5041
0.6024	0.8616	0.5218	1.0092	0.4534	1.2826	0.4331	1.5370
0.5614	0.8991	0.4870	1.0429	0.4243	1.3140	0.4060	1.5680
0.5181	0.9337	0.4500	1.0741	0.3930	1.3431	0.3765	1.5968
0.4725	0.9655	0.4109	1.1027	0.3596	1.3698	0.3449	1.6233
0.4251	0.9942	0.3699	1.1286	0.3244	1.3940	0.3114	1.6474
0.3758	1.0198	0.3273	1.1516	0.2875	1.4156	0.2762	1.6688
0.3250	1.0422	0.2832	1.1718	0.2491	1.4346	0.2396	1.6877
0.2729	1.0612	0.2379	1.1890	0.2095	1.4507	0.2016	1.7037
0.2197	1.0769	0.1916	1.2031	0.1689	1.4640	0.1626	1.7170
0.1655	1.0892	0.1444	1.2141	0.1274	1.4744	0.1227	1.7273
0.1107	1.0980	0.0966	1.2220	0.0853	1.4818	0.0822	1.7348
0.0555	1.1033	0.0484	1.2268	0.0427	1.4863	0.0412	1.7392
0.0000	1.1050	0.0000	1.2284	0.0000	1.4878	0.0000	1.7407

Table 3: Coordinates of optimal shapes for two interacting holes under remote biaxial loading $S_1 = -\frac{1}{2}S_2$ *for various* e/h *values.*

$S_1 = -\frac{1}{2}S_2$											
$e/h = 0.2754$ $K_t = 1.9410$ $h/w = 1.2235$		$e/h = 0.3224$ $K_t = 1.9156$ $h/w = 1.3288$		$e/h = 0.3834$ $K_t = 1.9015$ $h/w = 1.5159$		$e/h = 0.6162$ $K_t = 1.9022$ $h/w = 1.5497$		$e/h = 0.9499$ $K_t = 1.9151$ $h/w = 1.7862$		$e/h = 1.3406$ $K_t = 1.9477$ $h/w = 1.8398$	
x/h	y/h	x/h	y/h	x/h	y/h	x/h	y/h	x/h	y/h	x/h	y/h
0.0000	0.1377	0.0000	0.1612	0.0000	0.1916	0.0000	0.3081	0.0000	0.4750	0.0000	0.6703
0.0413	0.1382	0.0424	0.1621	0.0416	0.1925	0.0406	0.3088	0.0396	0.4755	0.0374	0.6706
0.0825	0.1397	0.0848	0.1647	0.0831	0.1953	0.0811	0.3110	0.0792	0.4769	0.0748	0.6715
0.1237	0.1425	0.1270	0.1689	0.1244	0.1997	0.1215	0.3144	0.1188	0.4793	0.1122	0.6731
0.1648	0.1465	0.1691	0.1749	0.1656	0.2056	0.1618	0.3188	0.1582	0.4826	0.1496	0.6751
0.2057	0.1519	0.2108	0.1824	0.2066	0.2126	0.2020	0.3242	0.1975	0.4876	0.1868	0.6788
0.2464	0.1588	0.2524	0.1911	0.2475	0.2200	0.2422	0.3302	0.2370	0.4905	0.2242	0.6776
0.2869	0.1668	0.2937	0.2010	0.2883	0.2285	0.2823	0.3361	0.2732	0.5068	0.2556	0.6981
0.3272	0.1757	0.3350	0.2107	0.3298	0.2300	0.3227	0.3403	0.2704	0.5442	0.2536	0.7355
0.3675	0.1843	0.3763	0.2205	0.3284	0.2703	0.3162	0.3787	0.2740	0.5815	0.2585	0.7726
0.4087	0.1876	0.3690	0.2605	0.3275	0.3107	0.3165	0.4176	0.2757	0.6190	0.2614	0.8099
0.3996	0.2290	0.3680	0.3012	0.3272	0.3511	0.3161	0.4566	0.2775	0.6564	0.2643	0.8472
0.3976	0.2713	0.3665	0.3419	0.3267	0.3914	0.3160	0.4956	0.2786	0.6939	0.2666	0.8845
0.3954	0.3136	0.3652	0.3825	0.3259	0.4318	0.3155	0.5345	0.2793	0.7314	0.2683	0.9219
0.3936	0.3559	0.3637	0.4232	0.3250	0.4721	0.3149	0.5735	0.2797	0.7689	0.2696	0.9593
0.3917	0.3982	0.3622	0.4639	0.3240	0.5125	0.3141	0.6124	0.2799	0.8064	0.2706	0.9967
0.3898	0.4405	0.3605	0.5045	0.3228	0.5528	0.3132	0.6513	0.2799	0.8439	0.2713	1.0341
0.3878	0.4828	0.3587	0.5451	0.3214	0.5932	0.3121	0.6903	0.2796	0.8814	0.2716	1.0716
0.3856	0.5251	0.3568	0.5858	0.3199	0.6335	0.3108	0.7292	0.2791	0.9189	0.2718	1.1090
0.3833	0.5673	0.3547	0.6264	0.3182	0.6738	0.3093	0.7681	0.2784	0.9564	0.2716	1.1464
0.3808	0.6096	0.3525	0.6670	0.3164	0.7142	0.3077	0.8071	0.2775	0.9939	0.2713	1.1838
0.3782	0.6519	0.3501	0.7077	0.3144	0.7545	0.3058	0.8460	0.2764	1.0314	0.2707	1.2212
0.3754	0.6941	0.3475	0.7483	0.3122	0.7948	0.3038	0.8849	0.2751	1.0689	0.2698	1.2587
0.3724	0.7363	0.3448	0.7889	0.3098	0.8351	0.3015	0.9238	0.2736	1.1063	0.2687	1.2961
0.3691	0.7786	0.3419	0.8294	0.3073	0.8754	0.2990	0.9626	0.2719	1.1438	0.2674	1.3335
0.3656	0.8208	0.3387	0.8700	0.3046	0.9156	0.2964	1.0015	0.2700	1.1813	0.2659	1.3709
0.3619	0.8629	0.3354	0.9105	0.3017	0.9559	0.2934	1.0404	0.2679	1.2187	0.2641	1.4082
0.3578	0.9051	0.3317	0.9511	0.2985	0.9961	0.2902	1.0792	0.2656	1.2561	0.2620	1.4456
0.3535	0.9472	0.3279	0.9916	0.2951	1.0364	0.2867	1.1180	0.2630	1.2935	0.2596	1.4830
0.3485	0.9892	0.3235	1.0320	0.2913	1.0766	0.2829	1.1567	0.2603	1.3309	0.2570	1.5203
0.3435	1.0313	0.3193	1.0725	0.2879	1.1168	0.2786	1.1955	0.2571	1.3683	0.2540	1.5576
0.3367	1.0731	0.3140	1.1128	0.2841	1.1570	0.2739	1.2341	0.2542	1.4057	0.2510	1.5949
0.3362	1.1154	0.3157	1.1535	0.2876	1.1972	0.2698	1.2729	0.2508	1.4430	0.2473	1.6321
0.2962	1.1294	0.2763	1.1560	0.2523	1.1897	0.2660	1.3116	0.2542	1.4804	0.2498	1.6695
0.2539	1.1300	0.2368	1.1563	0.2163	1.1900	0.2284	1.3054	0.2184	1.4737	0.2142	1.6670
0.2116	1.1332	0.1974	1.1581	0.1802	1.1902	0.1904	1.3066	0.1820	1.4740	0.1785	1.6677
0.1693	1.1348	0.1579	1.1593	0.1442	1.1907	0.1523	1.3069	0.1456	1.4741	0.1428	1.6686
0.1270	1.1361	0.1184	1.1602	0.1082	1.1911	0.1142	1.3074	0.1092	1.4745	0.1071	1.6694
0.0847	1.1370	0.0790	1.1608	0.0721	1.1914	0.0762	1.3078	0.0728	1.4747	0.0714	1.6699
0.0423	1.1375	0.0395	1.1611	0.0361	1.1915	0.0381	1.3080	0.0364	1.4749	0.0357	1.6702
0.0000	1.1377	0.0000	1.1612	0.0000	1.1916	0.0000	1.3081	0.0000	1.4750	0.0000	1.6703

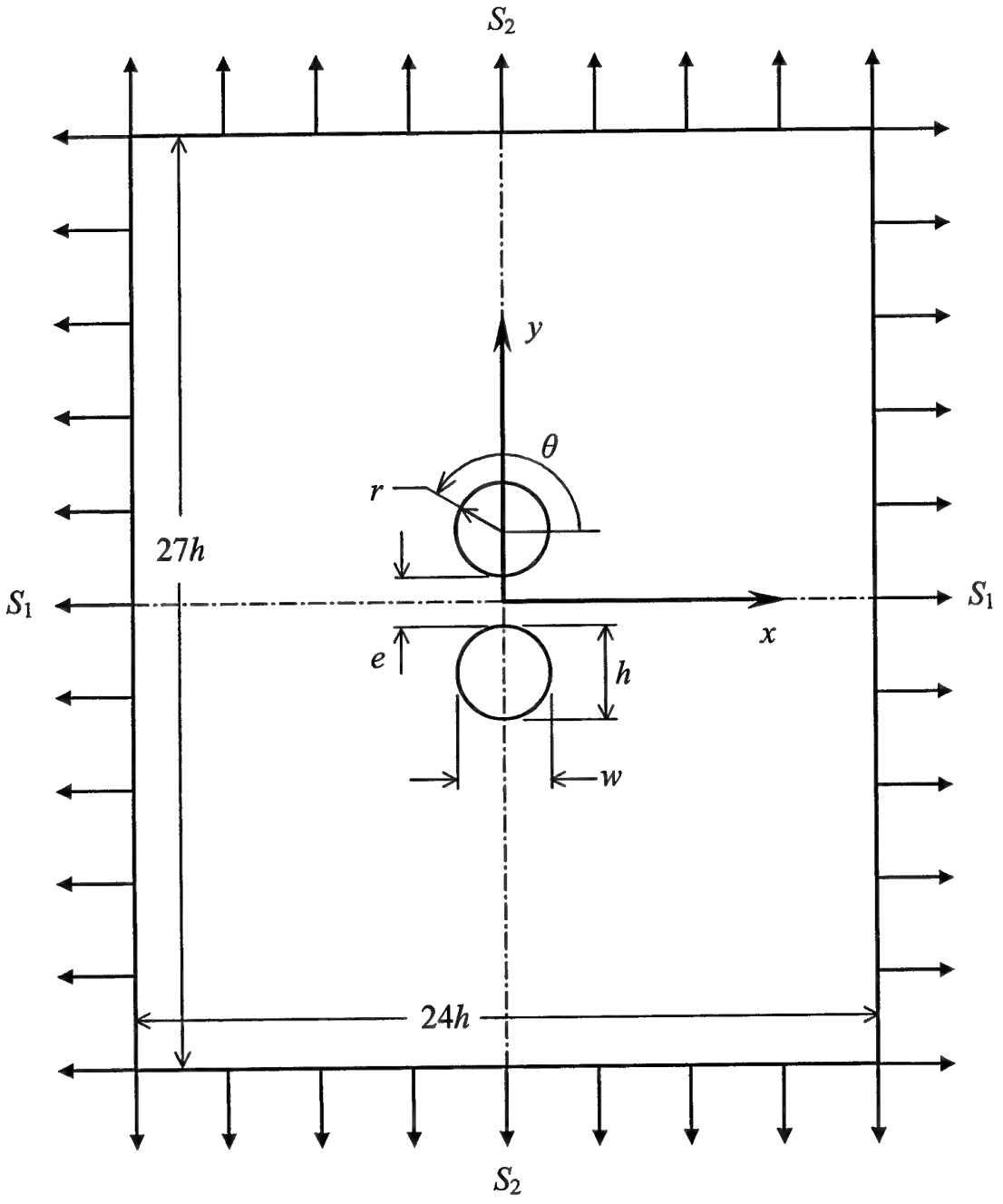

Fig. 1. Geometry and loading arrangement for a large rectangular plate containing two centrally located closely-spaced circular holes, each of height h *and width* w *(radius* r*), with minimum edge separation distance* e*, and a remote biaxial stress field* $y{:}x = S_2{:}S_1$.

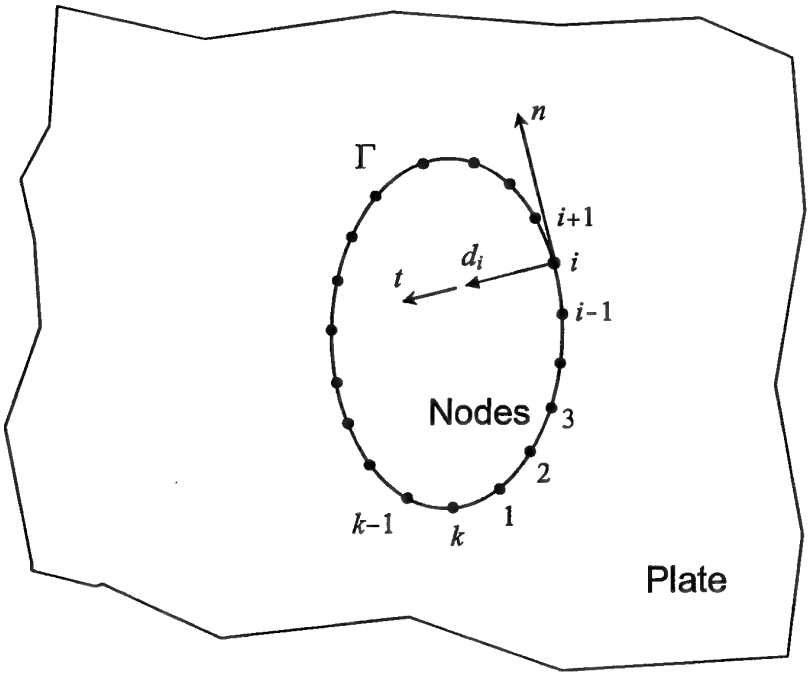

(a)

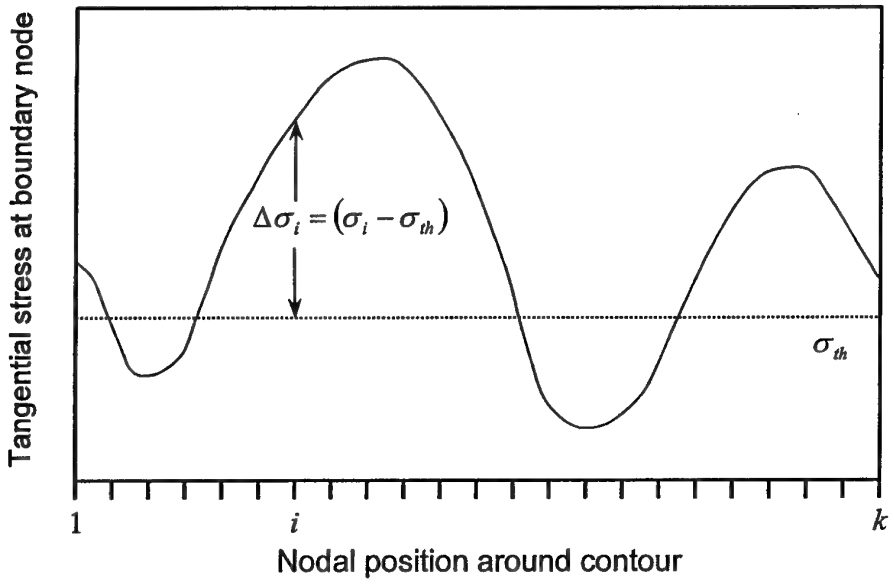

(b)

Fig. 2. Explanation of moving boundary method for case of an open hole in a remotely loaded plate. (a) Geometry and notation with hole boundary shape defined by k *nodes on contour* Γ. *(b) Typical tangential stress distribution around hole boundary contour.*

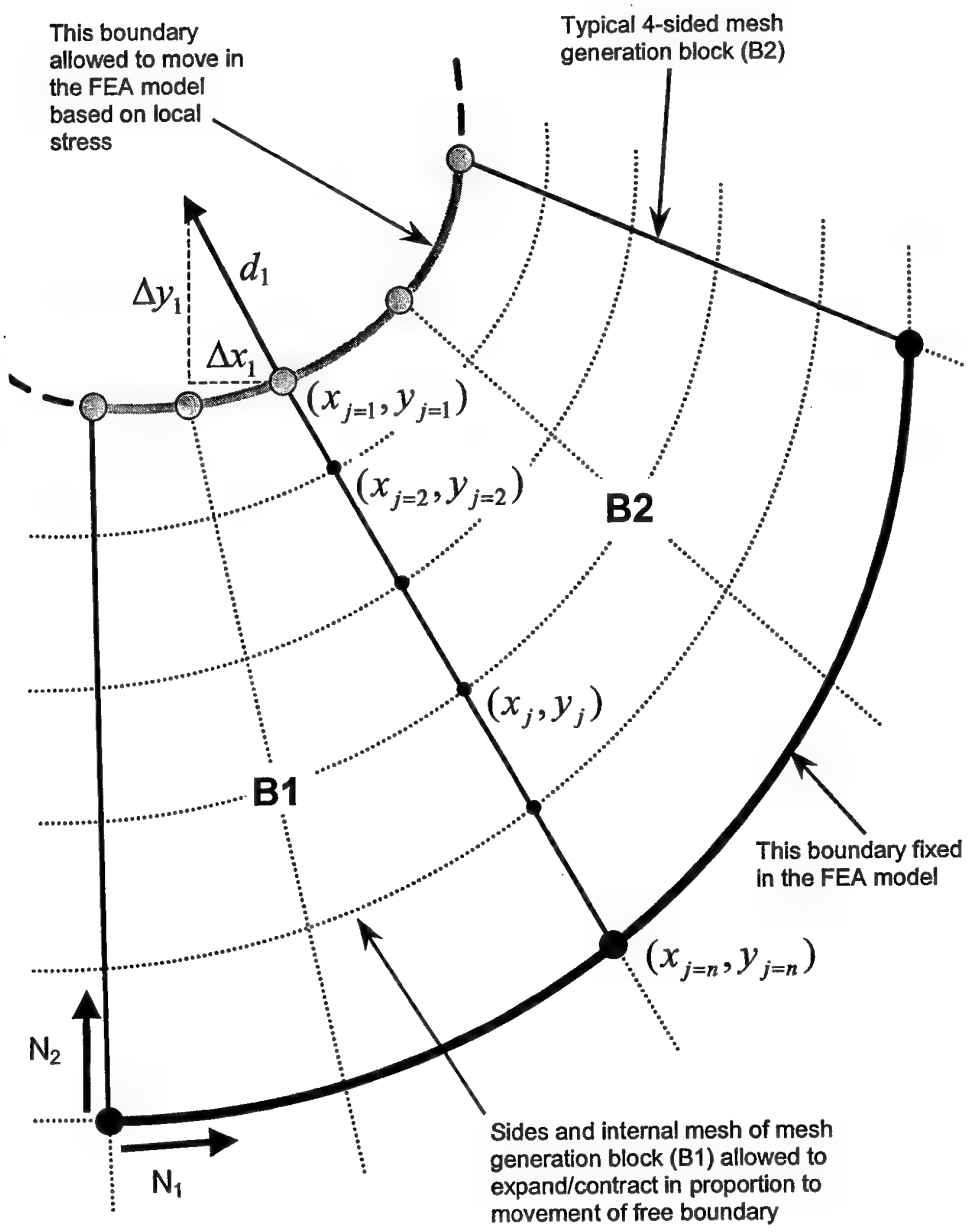

Fig. 3. Use of automatic mesh generation blocks (B1 and B2) to define FE mesh for shape optimisation of FEA model.

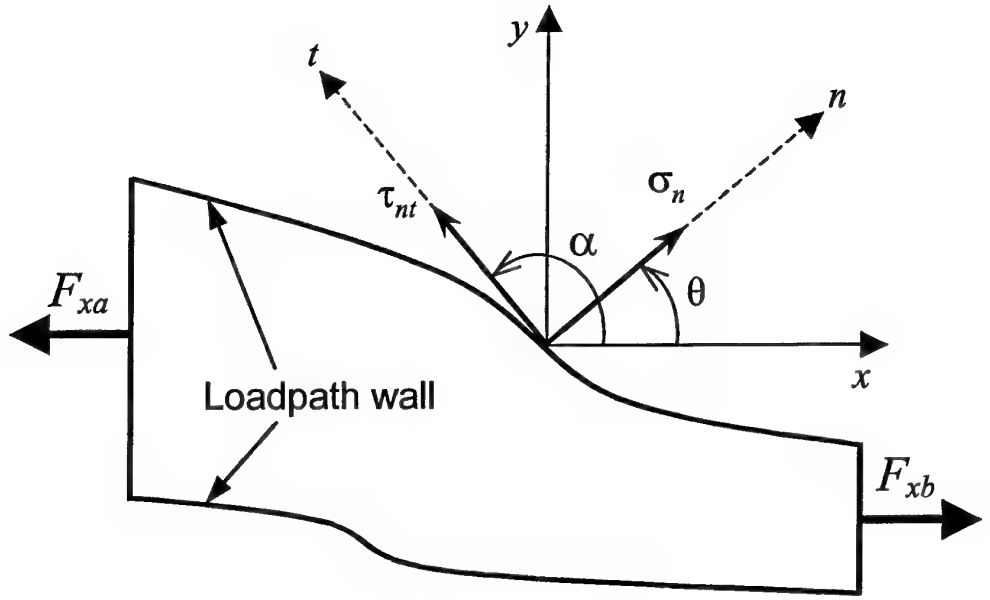

Fig. 4. Schematic of a force "stream tube" comprised of loadpath walls proposed by Kelly and Elsley (1993, 1995), shown for the resolved x-direction case.

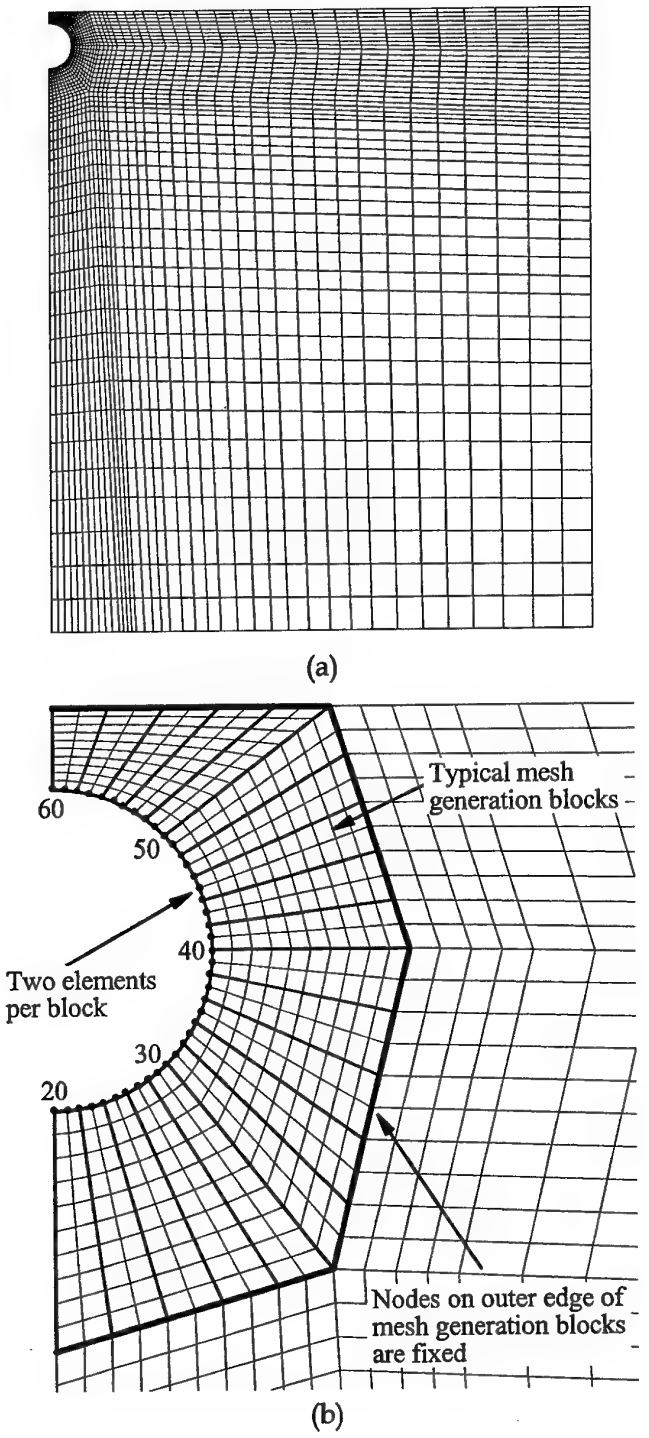

Fig. 5. Typical finite element mesh for ¼-symmetry model of large rectangular plate containing two closely-spaced circular holes. (a) Complete finite element mesh. (b) Detail of mesh around circular hole showing mesh generation blocks and node numbering around the hole boundary.

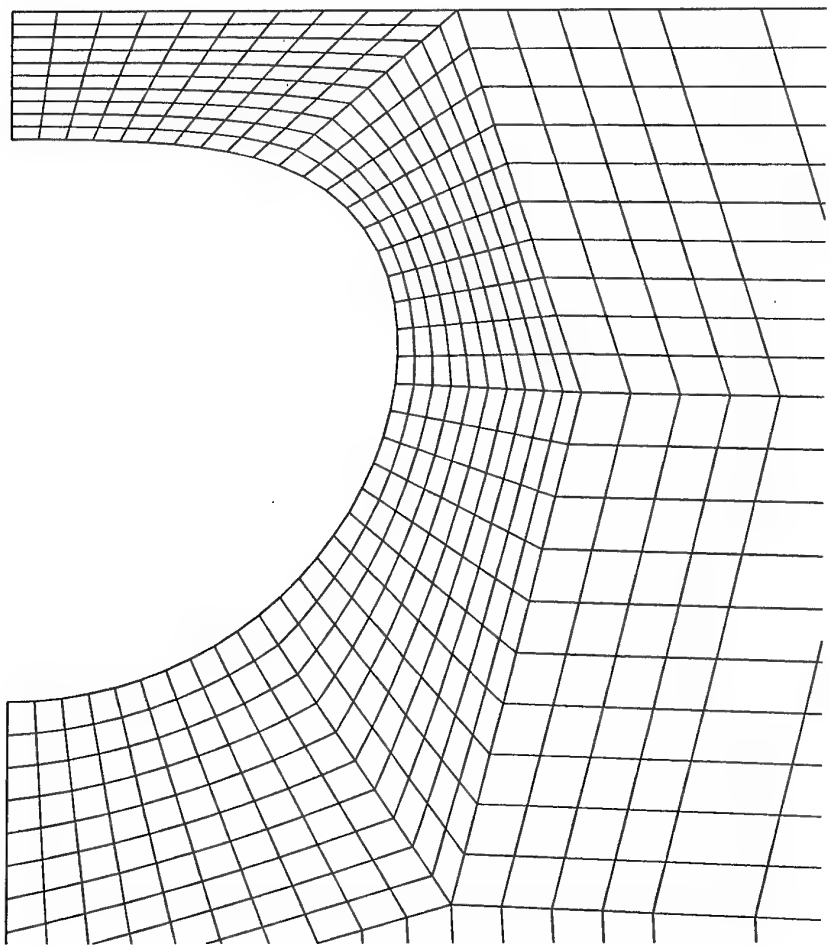

Fig. 6. Detail of mesh of ¼-symmetry FE model of optimal hole shape for two interacting holes under remote tensile biaxial loading $S_1 = S_2$ *with final* $e/h = 0.4568$.

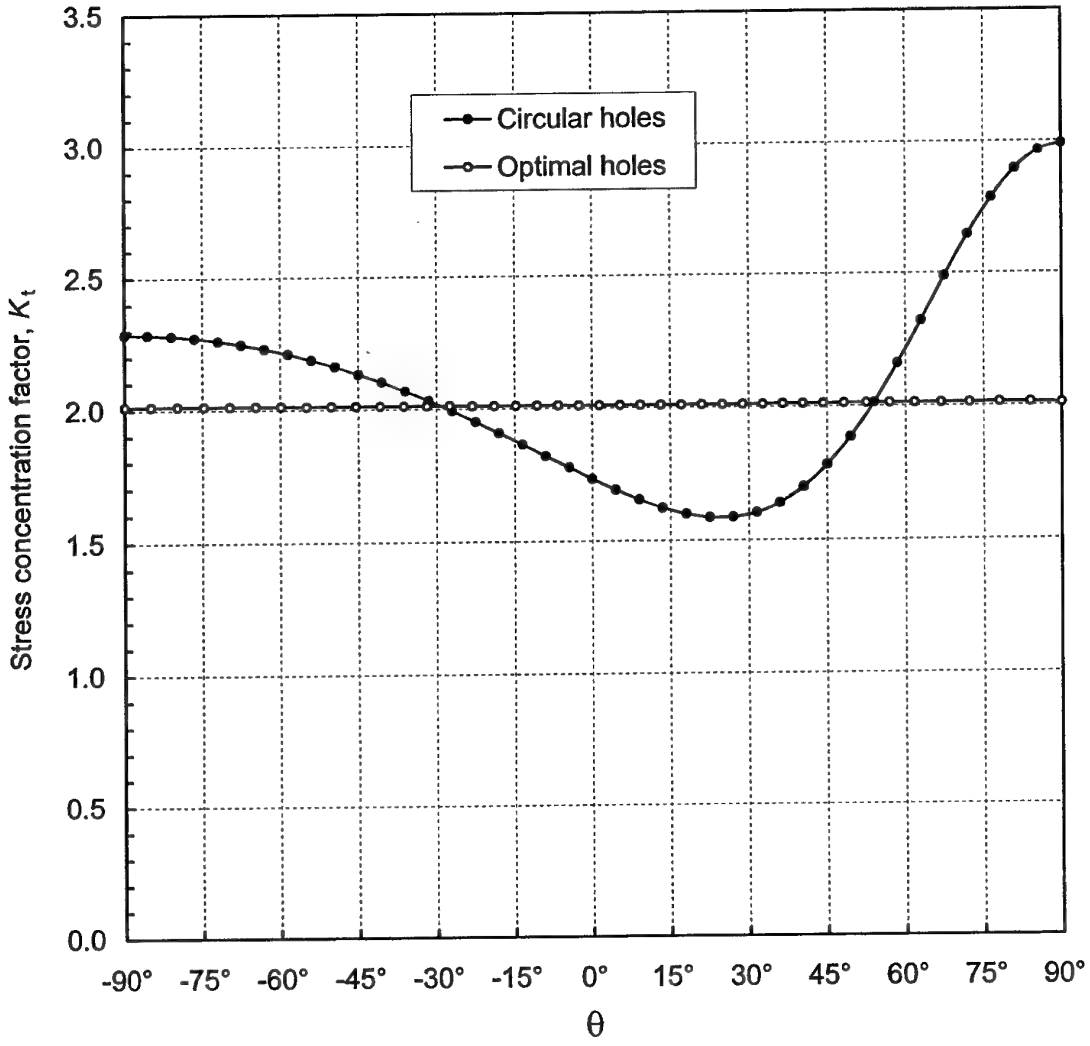

Fig. 7. Stress concentration factor around hole boundary of ¼-symmetry model of two interacting holes in a plate, for the case of a circular hole and an optimal hole for e/h = *0.4568 and remote tensile biaxial loading* $S_1 = S_2$.

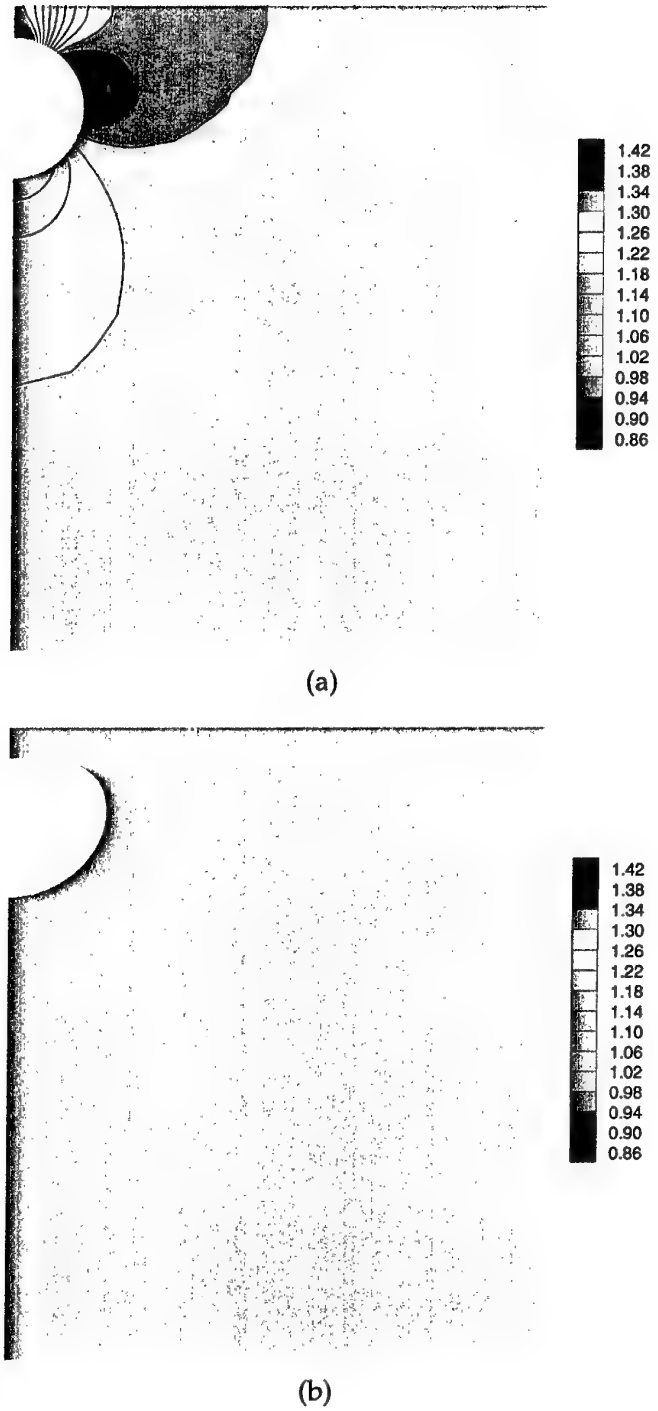

Fig. 8. Contour plots of normalised bulk stress $\hat{K}$ for ¼-symmetry model of two interacting holes in a plate for $e/h = 0.4568$ *and remote tensile biaxial loading* $S_1 = S_2$. *(a) Non-optimal circular hole. (b) Optimal hole.*

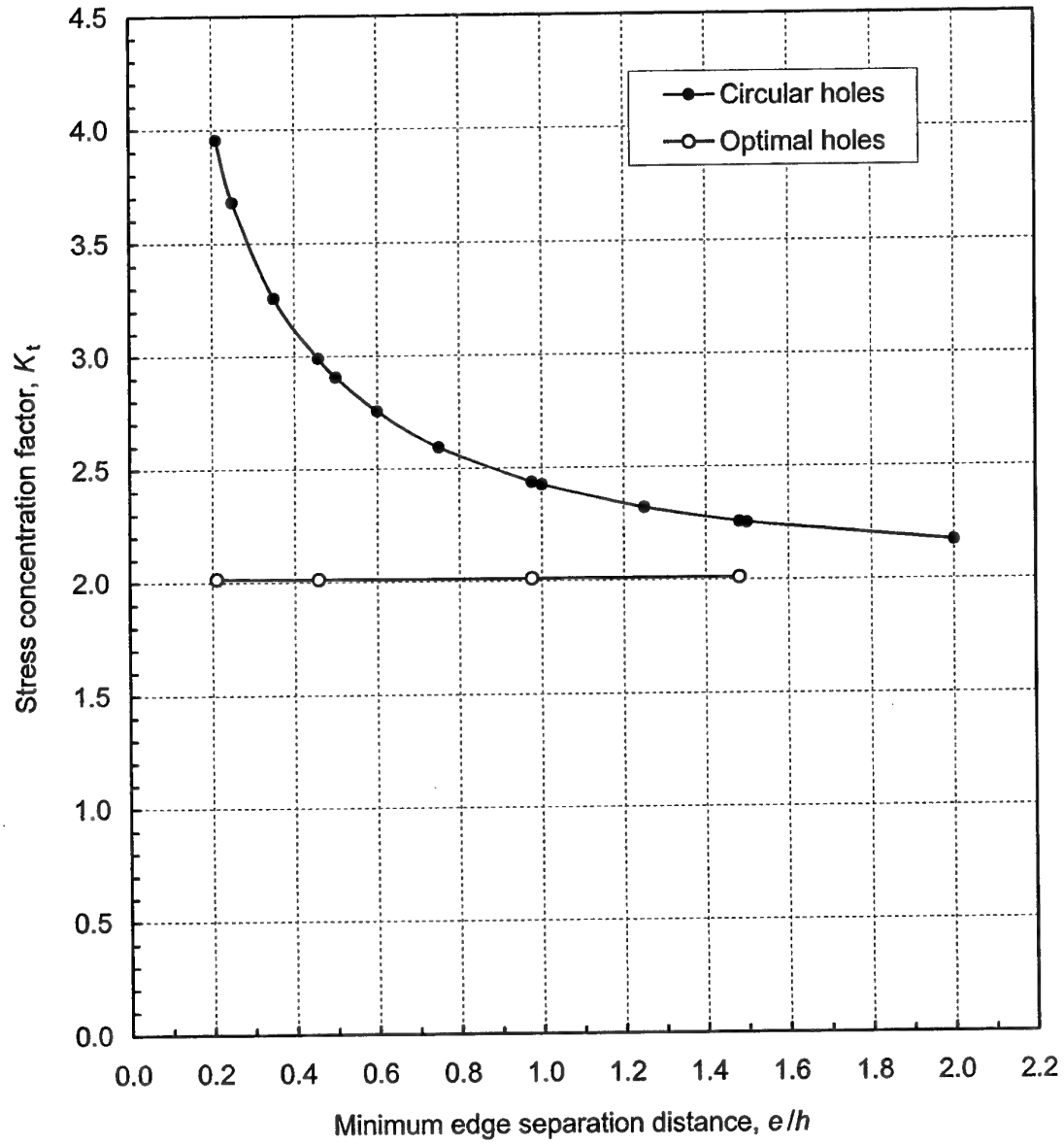

Fig. 9. Variation in stress concentration factor for two interacting circular and optimal holes in a large plate as a function of minimum edge separation distance between the two holes, e/h, *for tensile biaxial remote loading* $S_1 = S_2$.

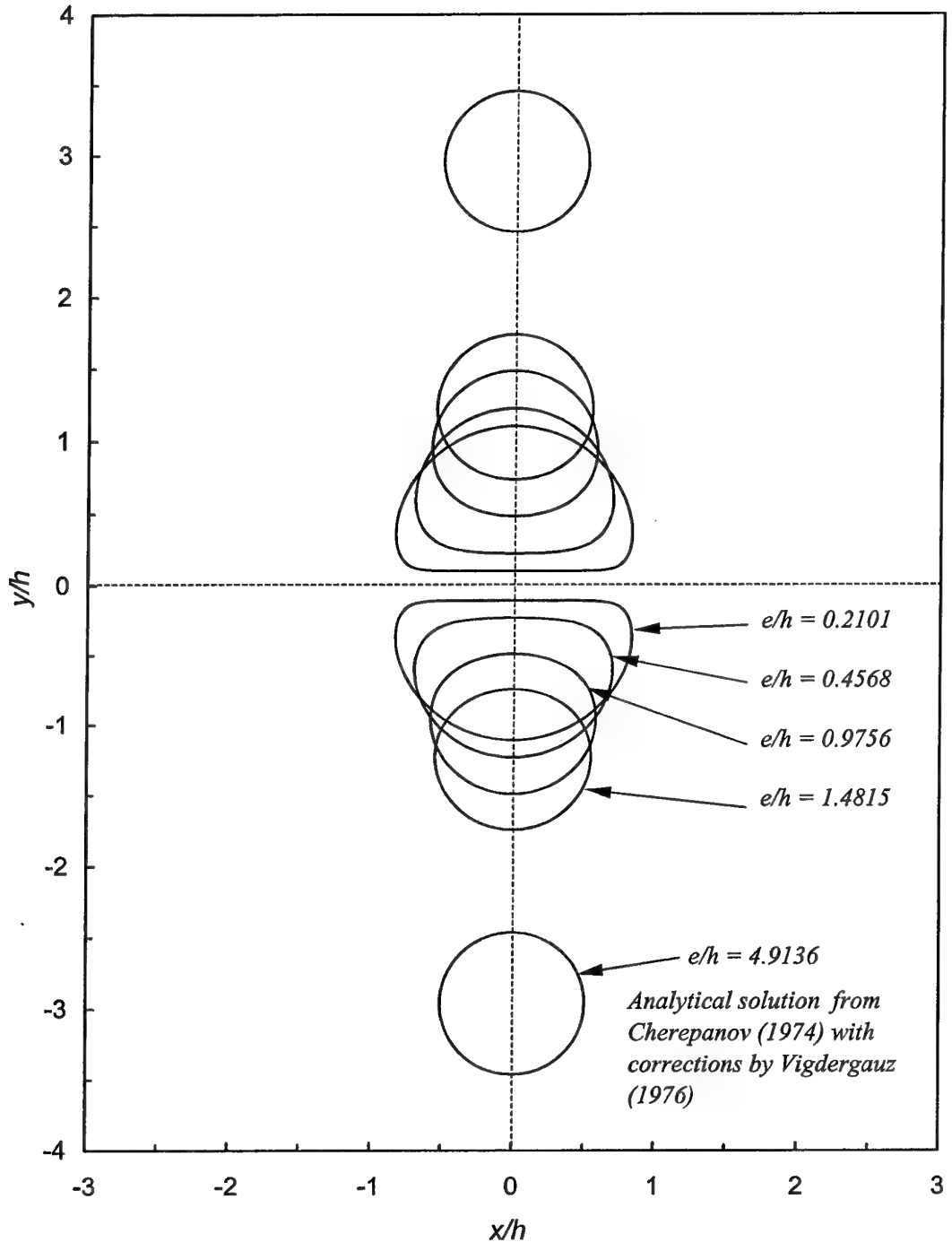

Fig. 10. Comparison of optimal shapes for two interacting holes in a large plate at different edge separations, e/h, for remote tensile biaxial loading $S_1 = S_2$.

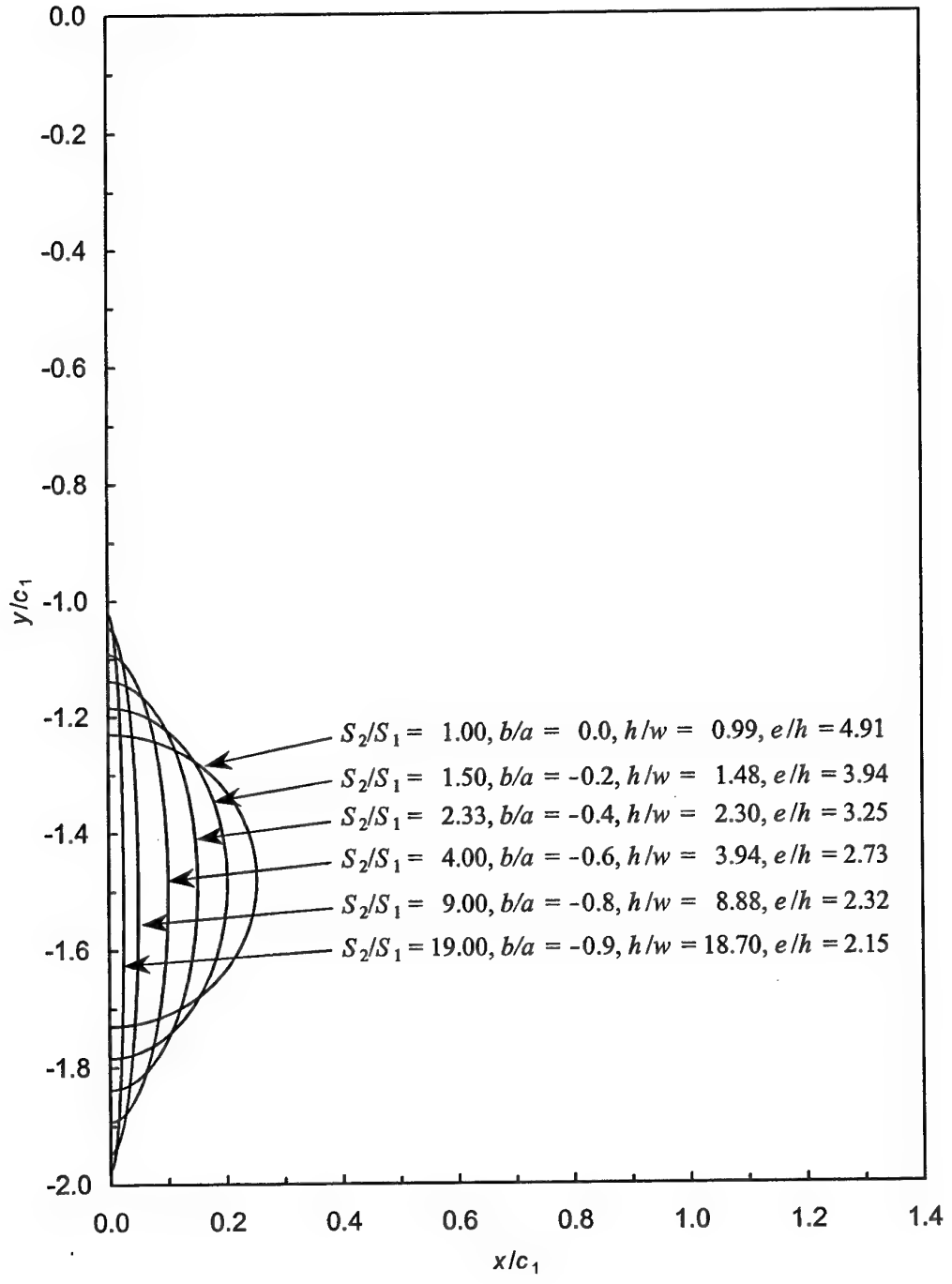

Fig. 11. ¼-symmetry representation of optimal hole shapes for two interacting holes in a plate calculated for various biaxial load ratios S_2/S_1 using the analytical solution by Cherepanov (1974) and incorporating corrections by Vigdergauz (1976).

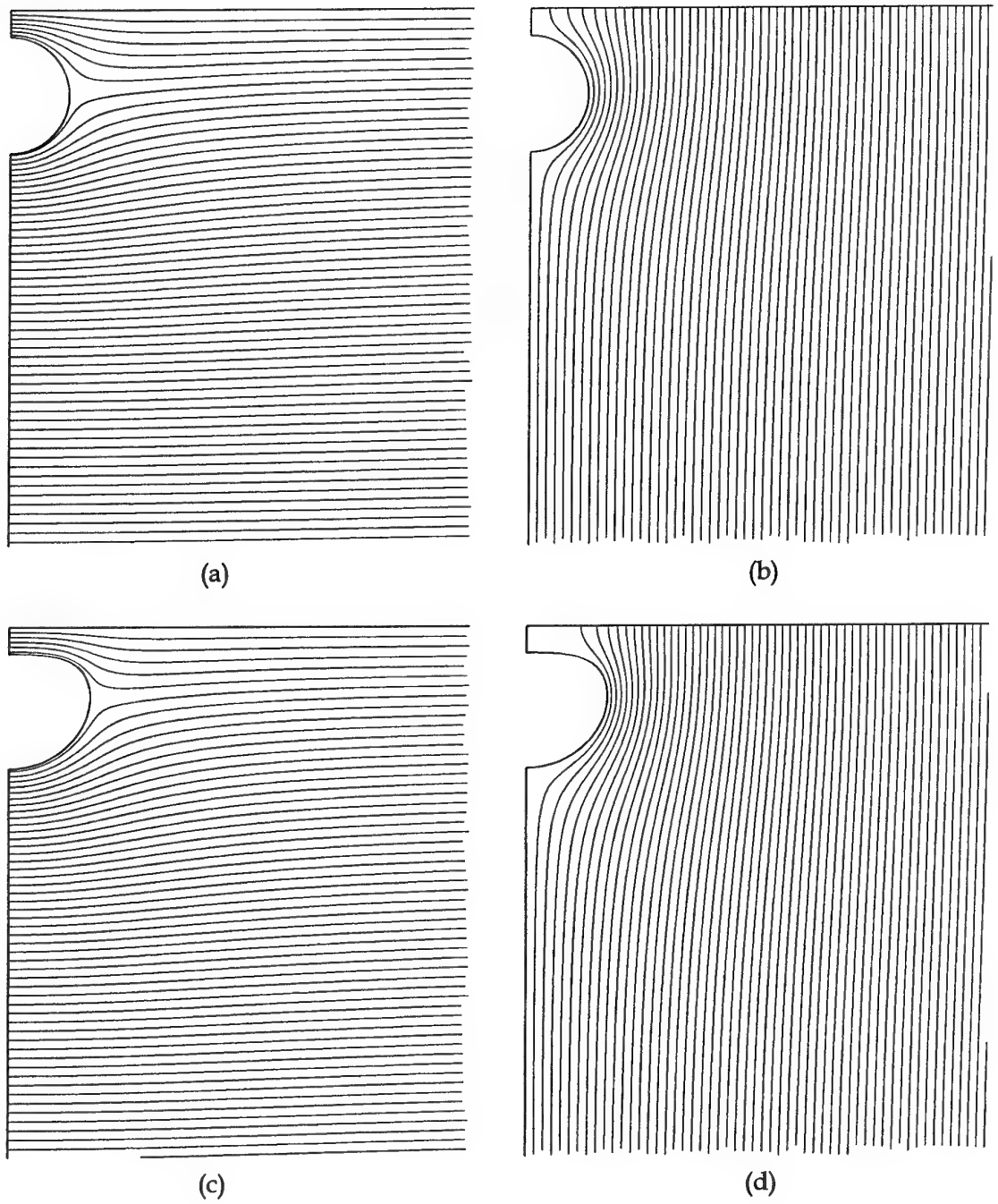

Fig. 12. Loadpaths for ¼-symmetry model of two interacting non-optimal circular holes and optimal hole shapes in a large plate for remote tensile field biaxial loading $S_1 = S_2$ *and* $e/h = 0.4568$. *(a) x-direction and (b) y-direction loadpaths for circular holes. (c) x-direction and (d) y-direction loadpaths for optimal holes.*

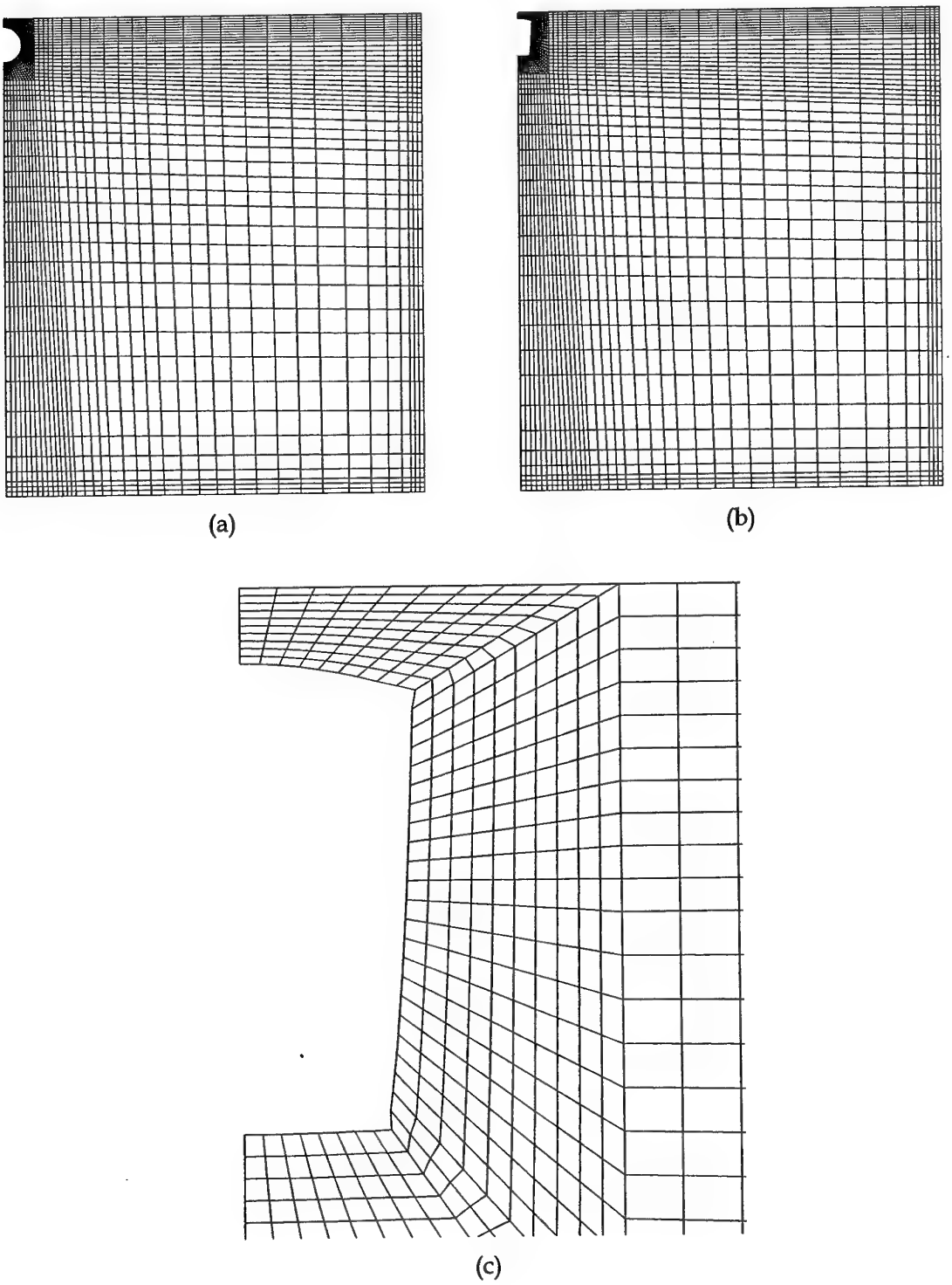

Fig. 13. Finite element mesh for ¼-symmetry model of large rectangular plate containing two closely-spaced holes for mixed biaxial field remote loading $S_1 = -\frac{1}{2}S_2$. *(a) Initial circular hole with* $e/h = 0.5$. *(b) Optimal hole with* $e/h = 0.3224$. *(c) Close-up view of mesh for optimal hole.*

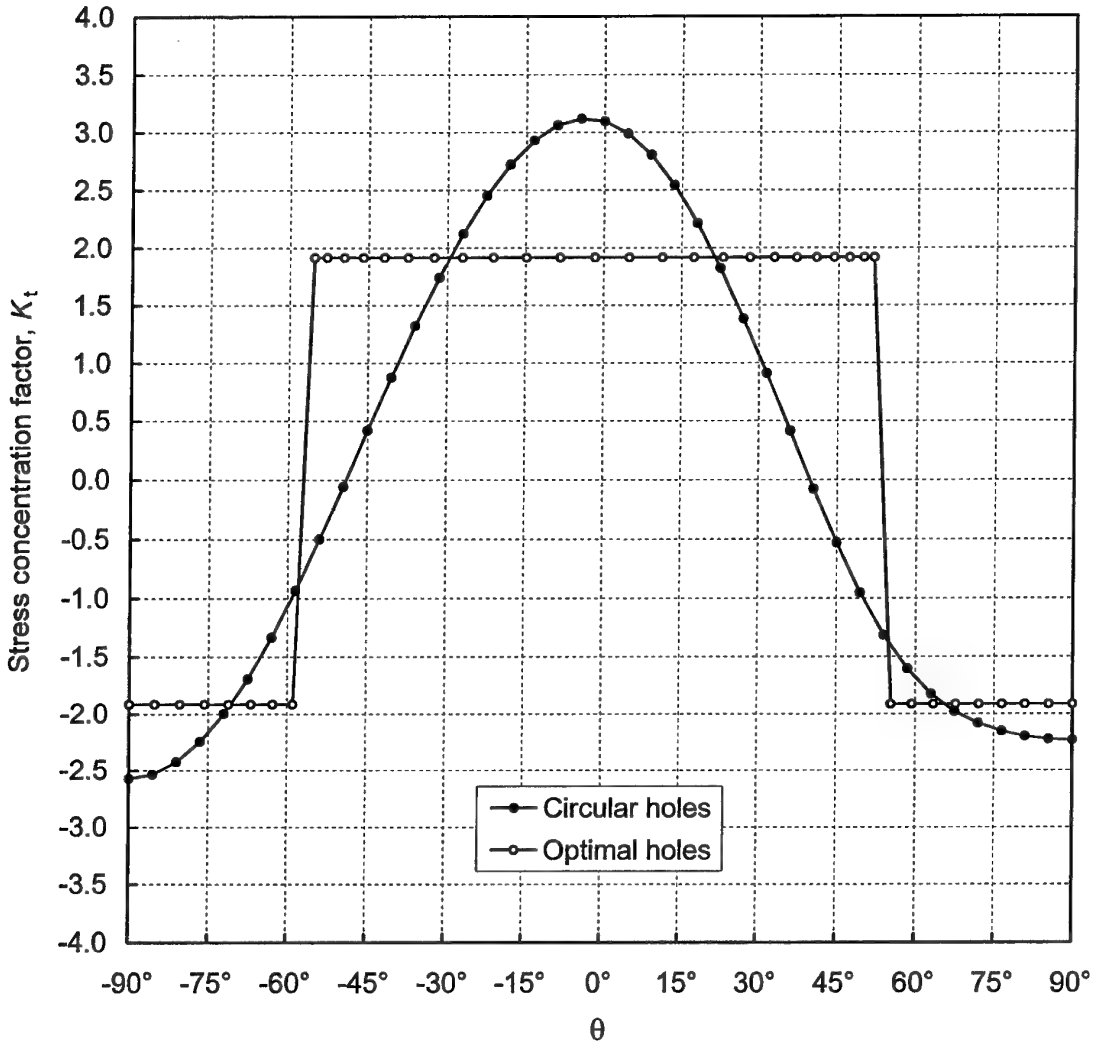

Fig. 14. Stress concentration factor around the hole boundary for two interacting holes in a large plate under mixed biaxial field remote loading $S_1 = -\frac{1}{2}S_2$ *and* $e/h = 0.3224$ *for a circular hole and the optimal hole.*

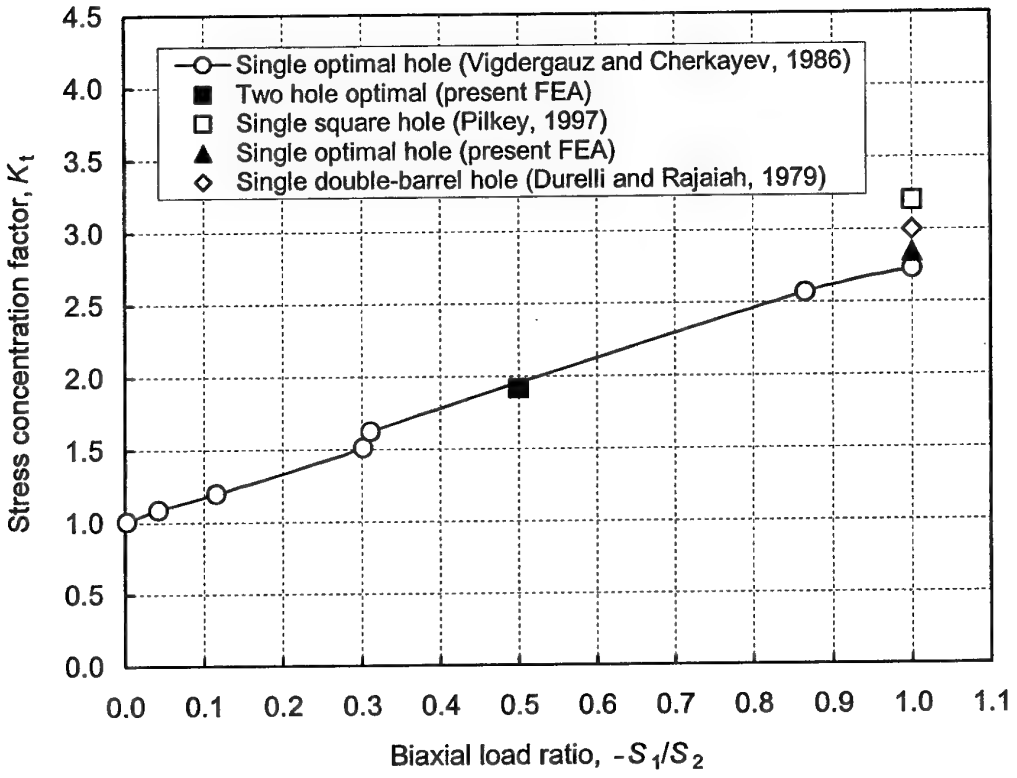

Fig. 15. Comparison of stress concentration factors for single optimal holes for different ratios of biaxial loading (mixed field), including results for two optimal interacting holes for $-S_1/S_2 = 1$ *and* $-S_1/S_2 = ½$.

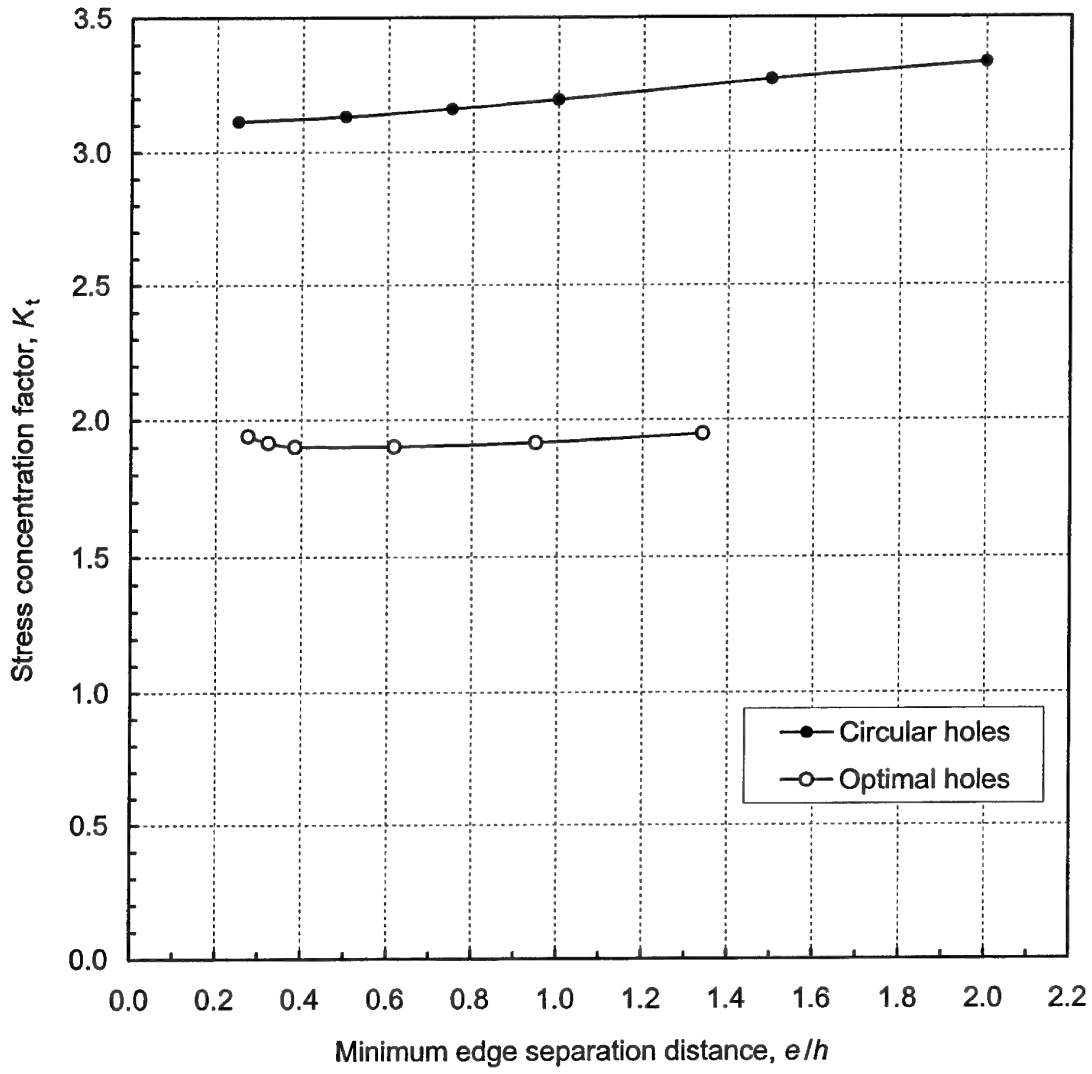

Fig. 16. Variation in stress concentration factor for two interacting circular and optimal holes as a function of minimum edge separation distance between the two holes, e/h, *for a large plate under remote loading* $S_1 = -½S_2$.

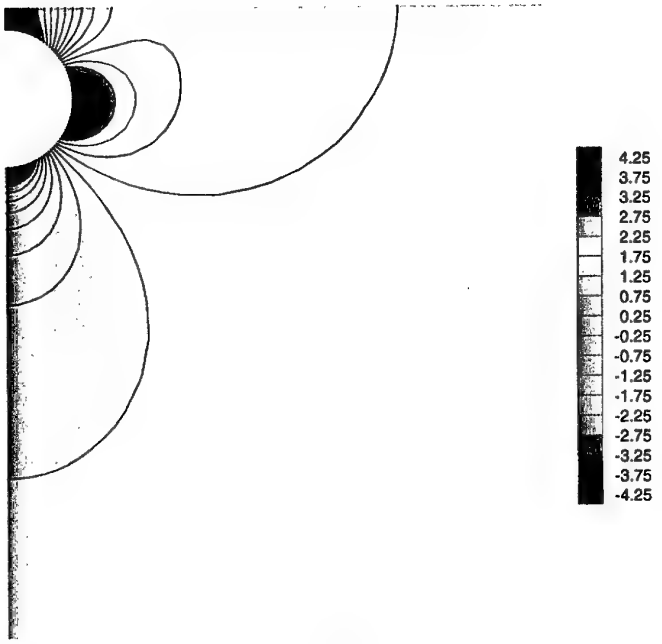

(a)

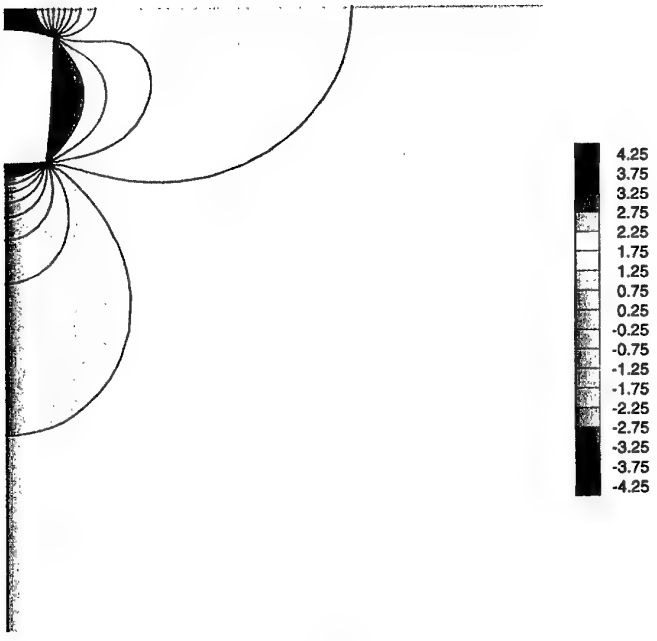

(b)

Fig. 17. Contours of normalised bulk stress $\hat{K}$ for ¼-symmetry model of two interacting holes in a large plate for mixed biaxial field remote loading $S_1 = -½S_2$ and e/h = 0.3224. (a) Non-optimal circular hole. (b) Optimal hole.

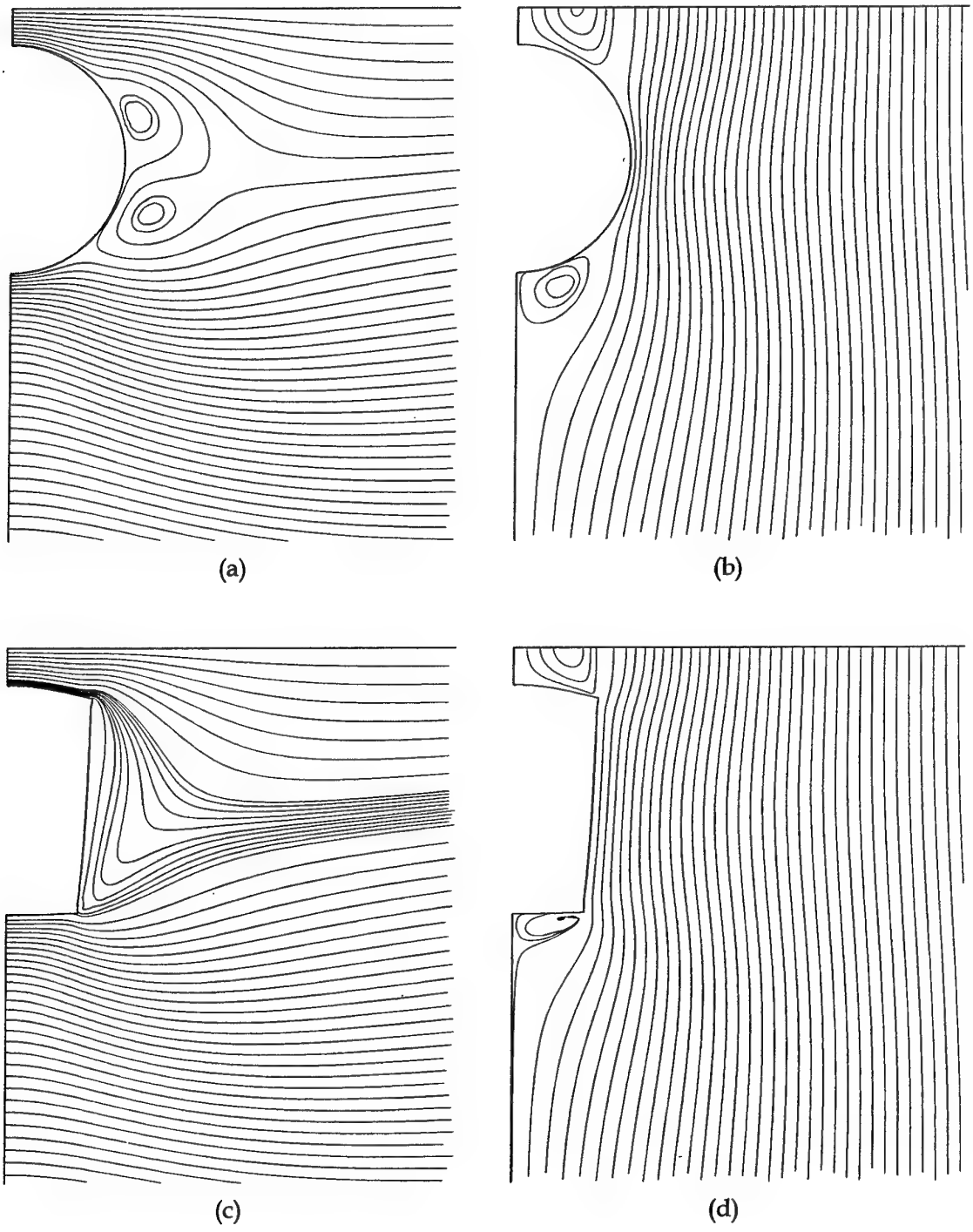

Fig. 18. Loadpaths for ¼-symmetry models of two interacting non-optimal circular holes and optimal holes in a large plate for mixed biaxial field remote loading $S_1 = -\frac{1}{2}S_2$ *and* $e/h = 0.3224$. *(a)* x*-direction loadpaths and (b)* y*-direction loadpaths for the circular hole. (c)* x*-direction loadpaths and (d)* y*-direction loadpaths for the optimal hole.*

DISTRIBUTION LIST

Shape Optimisation of Two Closely-Spaced Holes for Fatigue Life Extension

W. Waldman, M. Heller and L.R.F. Rose

DSTO-RR-0253

AUSTRALIA

DEFENCE ORGANISATION

Task sponsor
RAAF ASI DGTA

S&T Program
Chief Defence Scientist
FAS Science Policy
AS Science Corporate Management
Director General Science Policy Development
} shared copy
Counsellor Defence Science, London (Doc Data Sheet)
Counsellor Defence Science, Washington (Doc Data Sheet)
Scientific Adviser to MRDC Thailand (Doc Data Sheet)
Scientific Adviser Joint
Navy Scientific Adviser (Doc Data Sheet and distribution list only)
Scientific Adviser – Army (Doc Data Sheet and distribution list only)
Air Force Scientific Adviser
Director Trials

Platforms Sciences Laboratory
Chief of Air Vehicles Division (Doc Data Sheet and distribution list only)
Chief of Maritime Platforms Division (Doc Data Sheet and distribution list only)
Research Leader Aircraft Structures
Research Leader Aircraft Materials
Research Leader Propulsion Systems (Doc Data Sheet and distribution list only)
Research Leader Flight Systems (Doc Data Sheet and distribution list only)
Authors: W. Waldman (5 copies)
M. Heller (10 copies)
L.R.F. Rose (5 copies)
R. Kaye
S. Pitt
G. Chen
C. Wang
K.C. Watters
R. Callinan
L. Molent
M. Burchill

M. McDonald
R. Evans
K. Walker
R. Chester
B. Wicks
D. Lombardo
J. Hou
W. Hu
K. Sharp

DSTO Library and Archives
Library Fishermans Bend (Doc Data Sheet only)
Library Edinburgh, 1 copy
Australian Archives

Capability Systems Staff
Director General Maritime Development (Doc Data Sheet only)
Director General Aerospace Development (Doc Data Sheet only)

Knowledge Staff
Director General Command, Control, Communications and Computers (DGC4) (Doc Data Sheet only)

Air Force
ASI-LC
TLFM SQN Williamtown (Chief Engineer)

Army
ABCA National Standardisation Officer, Land Warfare Development Sector, Puckapunyal (4 copies)
SO (Science), Deployable Joint Force Headquarters (DJFHQ) (L), Enoggera, Queensland (Doc Data Sheet only)

Navy
SO (SCIENCE), COMAUSNAVSURFGRP, NSW (Doc Data Sheet and distribution list only)

Intelligence Program
DGSTA Defence Intelligence Organisation
Manager, Information Centre, Defence Intelligence Organisation

Defence Libraries
Library Manager, DLS-Canberra (Doc Data Sheet only)
Library Manager, DLS-Sydney West (Doc Data Sheet only)

UNIVERSITIES AND COLLEGES
Australian Defence Force Academy
Library
Head of Aerospace and Mechanical Engineering
Serials Section (M list), Deakin University Library, Geelong, Victoria
Hargrave Library, Monash University (Doc Data Sheet only)

Librarian, Flinders University

OTHER ORGANISATIONS
National Library of Australia
NASA (Canberra)

OUTSIDE AUSTRALIA

INTERNATIONAL DEFENCE INFORMATION CENTRES
US Defense Technical Information Center (2 copies)
UK Defence Technical Information Centre (2 copies)
Canada Defence Scientific Information Service
NZ Defence Information Centre

ABSTRACTING AND INFORMATION ORGANISATIONS
Library, Chemical Abstracts Reference Service
Engineering Societies Library, USA
Materials Information, Cambridge Scientific Abstracts, USA
Documents Librarian, The Center for Research Libraries, USA

INFORMATION EXCHANGE AGREEMENT PARTNERS
Acquisitions Unit, Science Reference and Information Service, UK
National Aerospace Laboratory, Japan
National Aerospace Laboratory, Netherlands

CANADA
Canadian Forces National Defence Headquarters
DAS ENG 6-3
Bombardier Inc, Canadair, Military Aircraft Division
N.N. Trong
CDSD Engineering Manager - J. Roussel
National Research Council, Institute for Aerospace Research, Ottawa
Library
B.M.K. Lee
D. Simpson

SPARES: 5 copies
TOTAL: 84 copies

DEFENCE SCIENCE AND TECHNOLOGY ORGANISATION DOCUMENT CONTROL DATA				1. PRIVACY MARKING/CAVEAT (OF DOCUMENT)
2. TITLE Shape Optimisation of Two Closely-Spaced Holes for Fatigue Life Extension				3. SECURITY CLASSIFICATION Document (U) Title (U) Abstract (U)
4. AUTHORS W. Waldman, M. Heller and L.R.F. Rose				5. CORPORATE AUTHOR Platforms Sciences Laboratory 506 Lorimer Street Fishermans Bend VIC 3207 Australia
6a. DSTO NUMBER DSTO-RR-0253	6b. AR NUMBER AR-012-771		6c. TYPE OF REPORT Research Report	7. DOCUMENT DATE May 2003
8. FILE NUMBER M1/9/1171	9. TASK NUMBER AIR 01/147	10. TASK SPONSOR RAAF ASI DGTA	11. NO. OF PAGES 40	12. NO. OF REFERENCES 42
13. URL on the World Wide Web http://www.dsto.defence.gov.au/corporate/reports/DSTO-RR-0253.pdf			14. RELEASE AUTHORITY Chief, Air Vehicles Division	

15. SECONDARY RELEASE STATEMENT OF THIS DOCUMENT

Approved for public release

OVERSEAS ENQUIRIES OUTSIDE STATED LIMITATIONS SHOULD BE REFERRED THROUGH DOCUMENT EXCHANGE, PO BOX 1500, EDINBURGH, SA 5111, AUSTRALIA.

16. DELIBERATE ANNOUNCEMENT

No limitation

17. CITATION IN OTHER DOCUMENTS

No limitation

18. DEFTEST DESCRIPTORS

shape, structural optimization, holes (openings), stress concentration, finite element analysis, fatigue life

19. ABSTRACT

This report presents a set of free-form optimal shapes and the corresponding stress concentration factors for two interacting closely-spaced holes in a large biaxially loaded plate. A range of interaction distances and two distinct biaxial loading cases are considered, namely tensile field (remote principal stresses have the same sign) or mixed field (remote principal stresses have the opposite sign). The optimal shapes are obtained using the finite element analysis based gradientless shape optimisation method recently developed in AVD. In a key unexpected result, which has not previously been identified, it has been discovered that the peak stress associated with the optimal holes is independent of the interaction distance, and that the peak stress is the same as that for an optimal single hole. In both stress field cases, the absolute value of the tangential stress is piecewise constant around the hole boundary. Compared to interacting closely-spaced circular holes, which are a common feature in aircraft structures producing significant stress concentrations that often lead to premature fatigue cracking, the optimal hole shapes provide for very large reductions in peak stress (typically greater than 30%), which results in a substantial increase in fatigue life. The free-form optimal shapes are presented in a tabular form that allows them to be used readily by designers. For the tensile biaxial field, the optimal shapes are smooth and non-circular. For the mixed biaxial field case, the optimal shapes are approximately rectangular with sharp corners and curved sides, and no stress singularities are present at the corners.